The Astrophysical Journal Letters, 995:L59 (18pp), 2025 December 20 https://doi.org/10.3847/2041-8213/ae2000

ZTF25abjmnps (AT2025ulz) and S250818k: A Candidate Superkilonova from a Subthreshold Subsolar Gravitational-wave Trigger

Mansi M. Kasliwal[1], Tomás Ahumada[1], Robert Stein[2,3,4], Viraj Karambelkar[1,5,41], Xander J. Hall[6], Avinash Singh[7], Christoffer Fremling[1,8], Brian D. Metzger[9,10], Mattia Bulla[11,12,13], Vishwajeet Swain[14], Sarah Antier[15], Marion Pillas[16], Malte Busmann[17], James Freeburn[18], Sergey Karpov[19], Aleksandra Bochenek[20], Brendan O'Connor[6], Daniel A. Perley[20], Dalya Akl[21,22], Shreya Anand[23,24,42], Andrew Toivonen[25], Sam Rose[1], Theophile Jegou du Laz[1], Chang Liu[26,27], Kaustav Das[1], Sushant Sharma Chaudhary[25], Tyler Barna[25], Aditya Pawan Saikia[14], Igor Andreoni[18], Eric C. Bellm[28], Varun Bhalerao[14], S. Bradley Cenko[3,4], Michael W. Coughlin[25], Daniel Gruen[17,29], Daniel Kasen[30,31], Adam A. Miller[26,27,32], Samaya Nissanke[33,34,35,36], Antonella Palmese[6], Jesper Sollerman[7], Niharika Sravan[37], G.C. Anupama[38], Smaranika Banerjee[7], Sudhanshu Barway[38], Joshua S. Bloom[24], Tomás Cabrera[6], Tracy Chen[39], Chris Copperwheat[20], Alessandra Corsi[40], Richard Dekany[8], Nicholas Earley[1], Matthew Graham[1], Patrice Hello[15], George Helou[39], Lei Hu[6], Yves Kini[36], Ashish Mahabal[1], Frank Masci[39], Tanishk Mohan[14], Natalya Pletskova[37], Josiah Purdum[8], Yu-Jing Qin[1], Nabeel Rehemtulla[26,27,32], Anirudh Salgundi[18], and Yuankun Wang[28]

[1] Division of Physics, Mathematics and Astronomy, California Institute of Technology, Pasadena, CA 91125, USA
[2] Department of Astronomy, University of Maryland, College Park, MD 20742, USA
[3] Joint Space-Science Institute, University of Maryland, College Park, MD 20742, USA
[4] Astrophysics Science Division, NASA Goddard Space Flight Center, MC 661, Greenbelt, MD 20771, USA
[5] Columbia University, 538 West 120th Street 704, MC 5255, New York, NY 10027, USA
[6] McWilliams Center for Cosmology and Astrophysics, Department of Physics, Carnegie Mellon University, 5000 Forbes Avenue, Pittsburgh, PA 15213, USA
[7] The Oskar Klein Centre, Department of Astronomy, Stockholm University, AlbaNova, SE-10691 Stockholm, Sweden
[8] Caltech Optical Observatories, California Institute of Technology, Pasadena, CA 91125, USA
[9] Department of Physics and Columbia Astrophysics Laboratory, Columbia University, New York, NY 10027, USA
[10] Center for Computational Astrophysics, Flatiron Institute, 162 5th Ave, New York, NY 10010, USA
[11] Department of Physics and Earth Science, University of Ferrara, via Saragat 1, I-44122 Ferrara, Italy
[12] INFN, Sezione di Ferrara, via Saragat 1, I-44122 Ferrara, Italy
[13] INAF, Osservatorio Astronomico d'Abruzzo, via Mentore Maggini snc, 64100 Teramo, Italy
[14] Department of Physics, Indian Institute of Technology Bombay, Powai, Mumbai 400076, India
[15] IJCLab, Univ Paris-Saclay, CNRS/IN2P3, Orsay, France
[16] Institut d'Astrophysique de Paris, Sorbonne Université and CNRS, UMR 7095, 98 bis bd Arago, 75014 Paris, France
[17] University Observatory, Faculty of Physics, Ludwig-Maximilians-Universität München, Scheinerstr. 1, 81679 Munich, Germany
[18] Department of Physics and Astronomy, University of North Carolina at Chapel Hill, Chapel Hill, NC 27599-3255, USA
[19] FZU—Institute of Physics of the Czech Academy of Sciences, Na Slovance 1999/2, CZ-182 21, Praha, Czech Republic
[20] Astrophysics Research Institute, Liverpool John Moores University, 146 Brownlow Hill, Liverpool, L3 5RF, UK
[21] New York University Abu Dhabi, PO Box 129188, Saadiyat Island, Abu Dhabi, UAE
[22] Center for Astrophysics and Space Science (CASS), New York University Abu Dhabi, Saadiyat Island, PO Box 129188, Abu Dhabi, UAE
[23] Kavli Institute for Particle Astrophysics and Cosmology, Stanford University, 452 Lomita Mall, Stanford, CA 94305, USA
[24] Department of Astronomy, University of California, Berkeley, CA 94720-3411, USA
[25] School of Physics and Astronomy, University of Minnesota, Minneapolis, MN 55455, USA
[26] Department of Physics and Astronomy, Northwestern University, 2145 Sheridan Road, Evanston, IL 60208, USA
[27] Center for Interdisciplinary Exploration and Research in Astrophysics (CIERA), Northwestern University, 1800 Sherman Ave, Evanston, IL 60201, USA
[28] DIRAC Institute, Department of Astronomy, University of Washington, 3910 15th Avenue NE, Seattle, WA 98195, USA
[29] Excellence Cluster ORIGINS, Boltzmannstr. 2, 85748 Garching, Germany
[30] Department of Physics and Department of Astronomy, University of California, Berkeley, CA 94720, USA
[31] Nuclear Science Division, Lawrence Berkeley National Laboratory, 1 Cyclotron Road, Berkeley, CA 94720, USA
[32] NSF-Simons AI Institute for the Sky (SkAI), 172 E. Chestnut St., Chicago, IL 60611, USA
[33] Deutsches Elektronen Synchrotron DESY, Platanenallee 6, 15738 Zeuthen, Germany
[34] Deutsches Zentrum für Astrophysik (DZA), Postplatz 1, 02826 Görlitz, Germany
[35] Institut für Physik und Astronomie, Universität Potsdam, Haus 28, Karl-Liebknecht-Str. 24/25, 14476, Potsdam, Germany
[36] Gravitation and Astroparticle Physics Amsterdam (GRAPPA), University of Amsterdam, 1098 XH Amsterdam, The Netherlands
[37] Department of Physics, Drexel University, Philadelphia, PA 19104, USA
[38] Indian Institute of Astrophysics, 2nd Block Koramangala, 560034, Bangalore, India
[39] IPAC, California Institute of Technology, 1200 E. California Blvd, Pasadena, CA 91125, USA
[40] Department of Physics and Astronomy, Johns Hopkins University, 3400 N. Charles Street Baltimore, MD 21218, USA
Received 2025 October 3; revised 2025 October 29; accepted 2025 November 3; published 2025 December 15

[41] NASA Hubble Fellow.
[42] LSST-DA Catalyst Postdoctoral Fellow.

Abstract

On 2025 August 18, the LIGO–Virgo–KAGRA collaboration reported gravitational waves from a subthreshold binary neutron star merger. If astrophysical, this event would have a surprisingly low chirp mass, suggesting that at least one neutron star was below a solar mass. The Zwicky Transient Facility mapped the coarse localization and discovered a transient, ZTF 25abjmnps (AT2025ulz), which was spatially and temporally coincident with the gravitational-wave trigger. The first week of follow-up suggested properties reminiscent of a GW170817-like kilonova. Subsequent follow-up suggests properties most similar to a young, stripped-envelope, Type IIb supernova. Although we cannot statistically rule out chance coincidence, we undertake due diligence analysis to explore the possible association between ZTF 25abjmnps and S250818k. Theoretical models have been proposed wherein subsolar neutron star(s) may form (and subsequently merge) via accretion-disk fragmentation or core fission inside a core-collapse supernova—i.e., a "superkilonova." Here, we qualitatively discuss our multi-wavelength dataset in the context of the superkilonova picture. Future higher-significance gravitational-wave detections of subsolar neutron star mergers with extensive electromagnetic follow-up would conclusively resolve this tantalizing multimessenger association.

Unified Astronomy Thesaurus concepts: Neutron stars (1108); Compact objects (288); Transient sources (1851); Core-collapse supernovae (304); Surveys (1671); Gravitational waves (678)

Materials only available in the online version of record: machine-readable tables

1. Introduction

Multimessenger astrophysics is the study of sources that are detected by at least two of four independent information messengers: electromagnetic radiation, gravitational waves (GWs), neutrinos, and cosmic rays. Until recently, our Sun and Supernova (SN) 1987A were the only two multimessenger sources from which both neutrinos and photons had been extensively studied. This past decade has seen tremendous progress in the study of multimessenger sources. The discovery of GW170817 (B. P. Abbott et al. 2017b)—a binary neutron star merger that was detected by both GW interferometers and telescopes across the entire electromagnetic spectrum—was a major breakthrough for the multimessenger field (see B. P. Abbott et al. 2017a and references therein, including D. A. Coulter et al. 2017; M. R. Drout et al. 2017; P. A. Evans et al. 2017; G. Hallinan et al. 2017; D. Kasen et al. 2017; M. M. Kasliwal et al. 2017; R. Margutti et al. 2017; E. Pian et al. 2017; S. J. Smartt et al. 2017; M. Soares-Santos et al. 2017; N. R. Tanvir et al. 2017; E. Troja et al. 2017). In the last 5 yr, multiple compelling electromagnetic counterparts have also been proposed to high-energy neutrinos: our own galaxy (Icecube Collaboration et al. 2023), active galactic nuclei (AGNs; M. Kadler et al. 2016; IceCube Collaboration et al. 2018, 2022; A. Plavin et al. 2020; R. Abbasi et al. 2022), tidal disruption flares (R. Stein et al. 2021; S. Reusch et al. 2022), and interacting hydrogen-poor SNe (R. Stein et al. 2025a). Separately, candidate counterparts to the highest-mass binary black hole mergers have also been proposed (M. J. Graham et al. 2020, 2023; T. Cabrera et al. 2024). Extensive searches in coarsely localized GW events of neutron star mergers have also led to more constraints on the nature of their electromagnetic counterparts (e.g., I. Andreoni et al. 2020; M. M. Kasliwal et al. 2020; K. Paterson et al. 2021; T. de Jaeger et al. 2022; T. Ahumada et al. 2024, 2025; L. Hu et al. 2025).

As we celebrate a decade since the discovery of the first GWs (B. P. Abbott et al. 2016), we acknowledge that GW events have opened our eyes to categories of sources that we did not even know existed. For example, no neutron star–black hole binary has yet been detected electromagnetically, and now over half a dozen have been detected in GWs (The LIGO Scientific Collaboration et al. 2025). Many facets of the black hole mass function have also come as a surprise, such as black holes in the upper mass gap and lower mass gap (The LIGO Scientific Collaboration et al. 2025). Now, the discovery of S250818k (Ligo Scientific Collaboration et al. 2025), the most plausible candidate to date for a merger of subsolar-mass neutron stars, could be another eye-opening discovery: subsolar compact objects could either be the long-awaited proof of existence of primordial black holes (Y. B. Zel'dovich & I. D. Novikov 1967; S. Hawking 1971; B. J. Carr 1975; G. F. Chapline 1975) or the first evidence of an entirely new stellar evolutionary pathway that could create such small neutron stars (A. L. Piro & E. Pfahl 2007; B. D. Metzger et al. 2024).

In this Letter, we present the discovery of an optical transient, ZTF 25abjmnps (AT2025ulz), and discuss the possibility of association with the GW trigger S250818k. In Section 2, we describe how the Zwicky Transient Facility (ZTF) promptly mapped the localization of the GW trigger S250818k and identified the transient ZTF 25abjmnps as a candidate counterpart amidst other unrelated transients. In Section 3, we present the extensive follow-up data taken by over a dozen telescopes worldwide in the optical and infrared wavelengths. In Section 4, we analyze the data in the context of kilonova and afterglow models. In Section 5, we analyze the data in the context of SN models and the literature sample of SNe. In Section 6, we examine whether the observed properties of AT2025ulz could be explained in the context of a theoretical model involving core fission or fragmentation in the disk of a core-collapse SN leading to the formation of subsolar neutron stars that subsequently merge, i.e., a superkilonova. The term "superkilonova" was first used to describe a theoretical model wherein a collapsar produces several solar masses of heavy elements by *r*-process nucleosynthesis (D. M. Siegel et al. 2022). Here, we propose to expand and generalize the use of the term "superkilonova" to more broadly include any core-collapse SN that has any kilonova-like *r*-process nucleosynthesis inside it (e.g., accretion-disk fragmentation and fissioning of the core, etc.). We conclude with forward-looking next steps on what could more conclusively prove or disprove the multimessenger association between such electromagnetic transients and GW events.

2. Discovery

On 2025 August 18 01:20:06.030 UTC, the LIGO–Virgo–KAGRA collaboration alerted the community (S. S. Chaudhary et al. 2024) to a compact binary merger candidate, S250818k, during the real-time processing of data from the LIGO Hanford

Observatory (H1), LIGO Livingston Observatory (L1), and Virgo Observatory (V1) (Ligo Scientific Collaboration et al. 2025). The low-latency false-alarm rate (FAR) was 2.1 yr^{-1}, a factor of just 2 higher than our nominal threshold of 1 yr^{-1} for automatically triggering follow-up. The low-latency estimate of the terrestrial probability was 70%. While this may seem high, we caution that low-latency estimates may improve significantly with offline analysis—specifically, the binary neutron star merger S231109ci had a low-latency FAR estimate of 13 yr^{-1} and a terrestrial probability of 96% but now has a published offline FAR estimate of 1 per 50 yr and is confirmed to be a binary neutron star (W. Niu et al. 2025). We also refer the reader to the analysis presented in J. H. Gillanders et al. (2025; see their Figure 1), based on M. Nicholl & I. Andreoni (2025), which shows the parameter space in which S250818k is closer to the locus of astrophysical GW triggers than terrestrial GW triggers.

If astrophysical in origin, S250818k is the only GW candidate event from online searches that has accompanying rapid parameter estimates in the subsolar-mass regime. The binned chirp mass estimate is 0.87 $M_{\odot}$ (highest probability), and at least one of the components is less than a solar mass at greater than 99% confidence (Ligo Scientific Collaboration et al. 2025). We note that previous searches of subsolar neutron star mergers have constrained rates (R. Abbott et al. 2022; LVK Collaboration et al. 2023). Targeted online searches for GWs emitted from subsolar mass are now underway, implemented in 2025 January, by the GstLAL and MBTA SSM search algorithms (C. Alléné et al. 2025; C. Hanna et al. 2025). To date, S250818k is the lowest-FAR candidate subsolar neutron star merger event.

When alerted by the `Fritz Marshal` instance of `Skyportal` (S. J. van der Walt et al. 2019; M. W. Coughlin et al. 2023), we deliberated on the points above and decided to manually trigger dedicated Target of Opportunity observations of S250818k with ZTF (E. C. Bellm et al. 2019; M. J. Graham et al. 2019; R. Dekany et al. 2020) using `snipergw`.[43] An observing plan was generated with `gwemopt` (M. W. Coughlin et al. 2018, 2019; M. Almualla et al. 2020) for the ZTF field grid, balancing the enclosed probability and observability for each individual ZTF field. We observed each field with three 300 s exposures (in the *g* band, *r* band, and then *g* band), to measure both the color and fade rate for all candidates. Our ZTF observations began promptly on 2025 August 18 04:02 UTC, approximately 2.7 hr after merger. We ultimately covered 33.1% of the reported localization region at least twice within the first 36 hr of merger (369.7 deg^2, correcting for chip gaps). With 300 s exposures, we reached a median depth of 21.85 (21.99) in the *g* band (*r* band). Our images were processed using the standard ZTF data processing pipeline (F. J. Masci et al. 2019), yielding individual transient alerts that were distributed to ZTF partnership brokers. The alerts were analyzed with `nuztf`, a software package developed to identify electromagnetic counterparts to neutrinos, GWs, and gamma-ray bursts (GRBs; R. Stein et al. 2023; R. D. Stein et al. 2025).

With the first night of data, `nuztf` selected 58 candidates with at least two detections and no detection history prior to merger. Of these candidates, ZTF 25abjmnps was immediately identified as the only candidate that appeared to be red and with a host galaxy photometric redshift consistent with the estimated merger distance (see Figure 1). The transient was reported to Transient Name Server (TNS) and assigned the name AT2025ulz (R. Stein 2025a), and it was also highlighted via a GCN Circular (R. Stein et al. 2025b). We repeated this analysis on subsequent nights. We also used independent search algorithms on ZTF data, such as ZTFReST (I. Andreoni et al. 2021) and `Fritz Marshal` filtering, to cross-validate our candidate list. Considering only sources detected within 72 hr of merger, there were a total 30,061 individual ZTF alerts in the 95% contour. Of these, 109 candidates were manually vetted using `Fritz Marshal`. We systematically ruled out all of the other candidates as either unrelated variable sources, sources too distant to be associated with S250818k, or sources with too slow photometric evolution. In some cases, additional photometry was obtained in order to confirm slow photometric evolution. The full list is given in Table 1, in Appendix B, alongside the rejection criterion for each candidate. Apart from ZTF 25abjmnps, no other plausible counterparts were found in our data. An independent mapping and search by the Pan-STARRS1 (PS1) survey reports no other candidate counterpart to S250818k (J. H. Gillanders et al. 2025; S. J. Smartt et al. 2025). In Appendix B, we discuss some candidates discussed in J. H. Gillanders et al. (2025) and N. Franz et al. (2025) as comparably compelling (or even higher-ranked by their metric) to ZTF 25abjmnps—our conclusion remains that ZTF 25abjmnps is the only plausible candidate counterpart to S250818k.

3. Follow-up

Fortuitously, ZTF 25abjmnps was located in the overlap region between two ZTF fields, yielding a total of six ZTF observations in the first night. After the identification of ZTF 25abjmnps as a candidate counterpart, extensive photometric follow-up was undertaken by the Fraunhofer Telescope at Wendelstein Observatory (FTW), Liverpool Telescope (LT), Canada–France–Hawaii Telescope (CFHT), Gemini Observatory Two-meter Twin Telescope (TTT), 2 m Himalayan Chandra Telescope (HCT), Palomar 60 inch/Spectral Energy Distribution Machine (SEDM), and Keck I/Low Resolution Imaging Spectrometer (LRIS) in the optical and Keck I/Multi-Object Spectrometer For Infra-Red Exploration (MOSFIRE), P200/Wide Field Infrared Camera (WIRC), FTW, Astrophysics Research Consortium (ARC) 3.5 m/Near-Infrared Camera and Fabry–Perot Spectrometer (NICFPS), and WINTER in the infrared. For spectroscopic follow-up, we used Keck I/LRIS, Gemini North/Gemini Multi-Object Spectrograph (GMOS), and MMT/Binospec. Details about the follow-up telescopes and data analysis are provided in Appendix A. The follow-up effort was coordinated via the `Fritz Marshal` instance of `Skyportal`.

To carefully cross-calibrate the photometry self-consistently across multiple telescopes, we took the following steps. For subtraction, all telescopes used the same set of templates: Legacy Survey DR10 images (A. Dey et al. 2019) for the *g* band and *z* band, the PS1 image for the *i* band, and archival MegaCam UNIONS survey images[44] for the *r* band. For zero-point calculations, all telescopes used a common set of calibration stars from the PS1 catalog. As the object is located on top of a bright host galaxy, and the passbands of the science images and templates are not exactly the same, the galaxy is

[43] https://github.com/robertdstein/snipergw

[44] www.skysurvey.cc/releases/

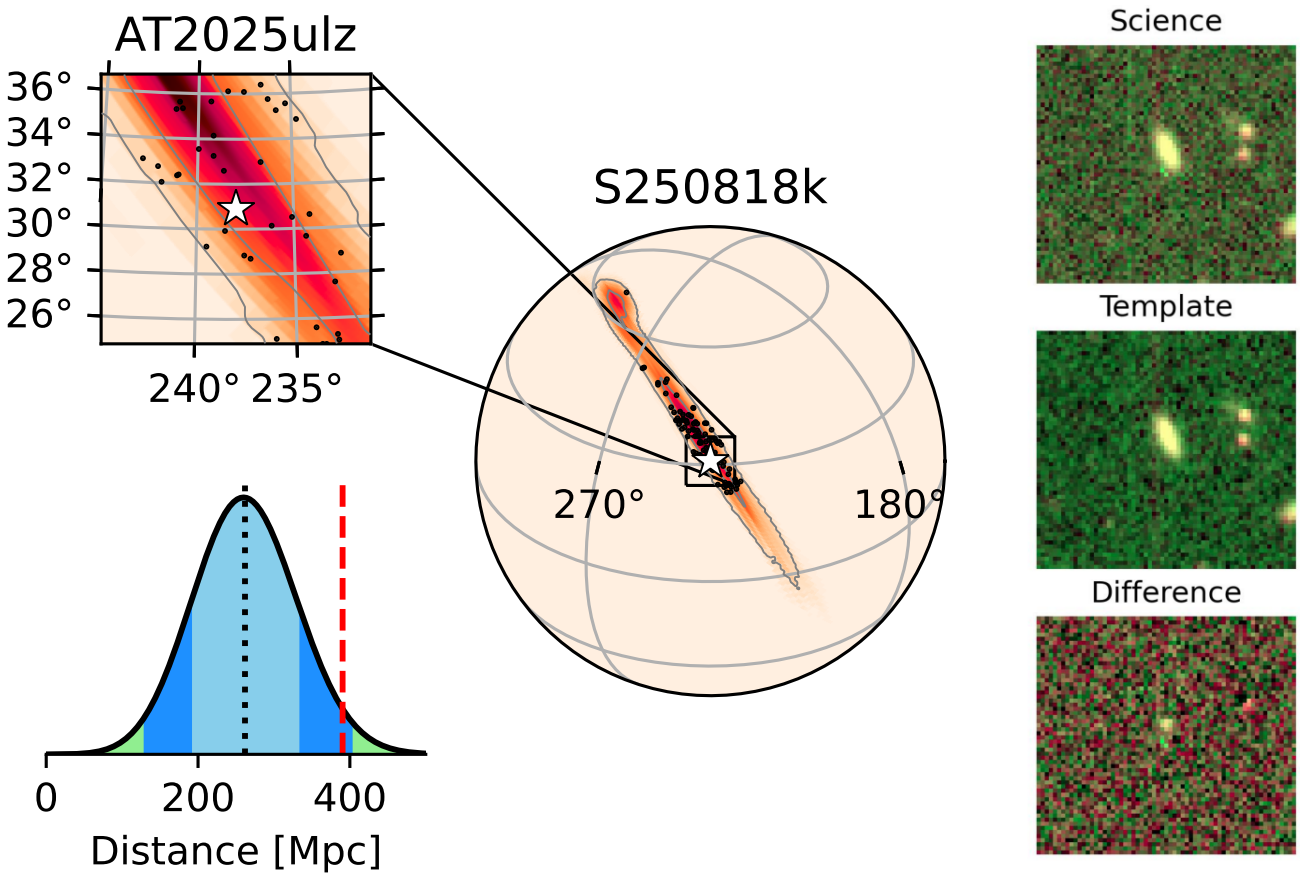

Figure 1. The discovery of ZTF 25abjmnps. Upper left: zoomed-in sky map of S250818k, with the 50% and 95% contours marked by gray lines, and the position of ZTF 25abjmnps marked by a white star. The other excluded ZTF candidates are marked by black dots. ZTF 25abjmnps lies within the central 50% region, close to the center. Center: zoomed-out sky map of S250818k. Lower left: line-of-sight distance at the position of ZTF 25abjmnps. The median GW distance (262 Mpc) at the location of ZTF 25abjmnps is illustrated with the vertical dotted black line, and the shaded regions correspond to the $\pm1\sigma$, $\pm2\sigma$, and $\pm3\sigma$ regions. The luminosity distance of ZTF 25abjmnps is illustrated with the dashed red line and lies within 2σ of the median value. Right: false-color ZTF discovery image of ZTF 25abjmnps in the *g* band and *r* band (top), alongside the template reference image (center) and difference image (bottom). Differencing yields a clean PSF-like excess in both filters at the location of the transient.

not always cleanly subtracted, leading to subtraction residuals that might impact the photometry. To account for this, we reduced the aperture size, to reduce the contribution from biased background estimation inside it. Our error estimate includes both statistical error and a systematic error floor (0.1 mag minimum when fainter than 21.5 mag; 0.05 mag minimum when brighter than 21.5 mag). The systematic error floor captures the measurement variations when changing the aperture size and roughly corresponds to the scatter due to filter mismatch. A list of all photometry is given in Table 2 and shown in Figure 2. To obtain smooth interpolations of the light curves, we used Gaussian Process (GP) regression, as implemented in `scikit-learn`. The GP was applied in logarithmic time space with a Matérn ($\nu = 2.5$) kernel, which provides a flexible yet smooth representation of the light-curve evolution while naturally incorporating photometric uncertainties. The GP fit is also shown in Figure 2.

To correct for reddening, we consider both Galactic and intrinsic host extinction. We estimate and correct for Galactic extinction using dust maps from E. F. Schlafly & D. P. Finkbeiner (2011). The presence of narrow Na I D lines from the host galaxy in the spectrum can be a good proxy for host galaxy reddening (D. Poznanski et al. 2012; M. D. Stritzinger et al. 2018). Specifically, the equivalent width of the Na I D_1 and D_2 lines can be related to the extinction by the following empirical relation: $A_v^{\rm host} = 0.78(\pm0.15)\,{\rm EW}_{\rm Na\,I\,D}$ (M. D. Stritzinger et al. 2018). Using the LRIS spectrum taken on UT 2025 August 25, we measure ${\rm EW}_{\rm Na\,I\,D}$ and calculate $E(B-V) \approx 0.29$ mag and $A_v^{\rm host} \approx 0.89$ mag, adopting the coefficients from E. F. Schlafly & D. P. Finkbeiner (2011; i.e., $R_v = 3.1$), who assumed a reddening law from E. L. Fitzpatrick (1999). For this, we opt to use a spectrum where the object is placed in the slit, rather than the center of the host galaxy, to probe the extinction of the transient's local environment. We caution that since low-resolution spectra are being used, this estimate is best used as an upper limit on the extinction (D. Poznanski et al. 2012).

In order to derive a redshift from the spectra, we use multiple host galaxy emission lines that yield $z = 0.0848$ or 399.4 Mpc, which we adopt throughout. To correct for host galaxy contamination in the transient spectra, we compare two approaches: scale and subtract an archival host galaxy spectrum versus model the host galaxy light using the method described in C. Liu & A. A. Miller (2025). We find using an archival host spectrum from the DESI survey (X. J. Hall 2025; X. J. Hall et al. 2025b) to yield overall less noisy results, and we show these in the spectral collage in Figure 3. In a few months, we plan to get a host galaxy spectrum exactly at the transient location after the transient has faded and expect that to yield the cleanest results. Host galaxy light subtraction is particularly challenging, as the transient is located on top of an active star-forming region in the galaxy. Therefore, to facilitate

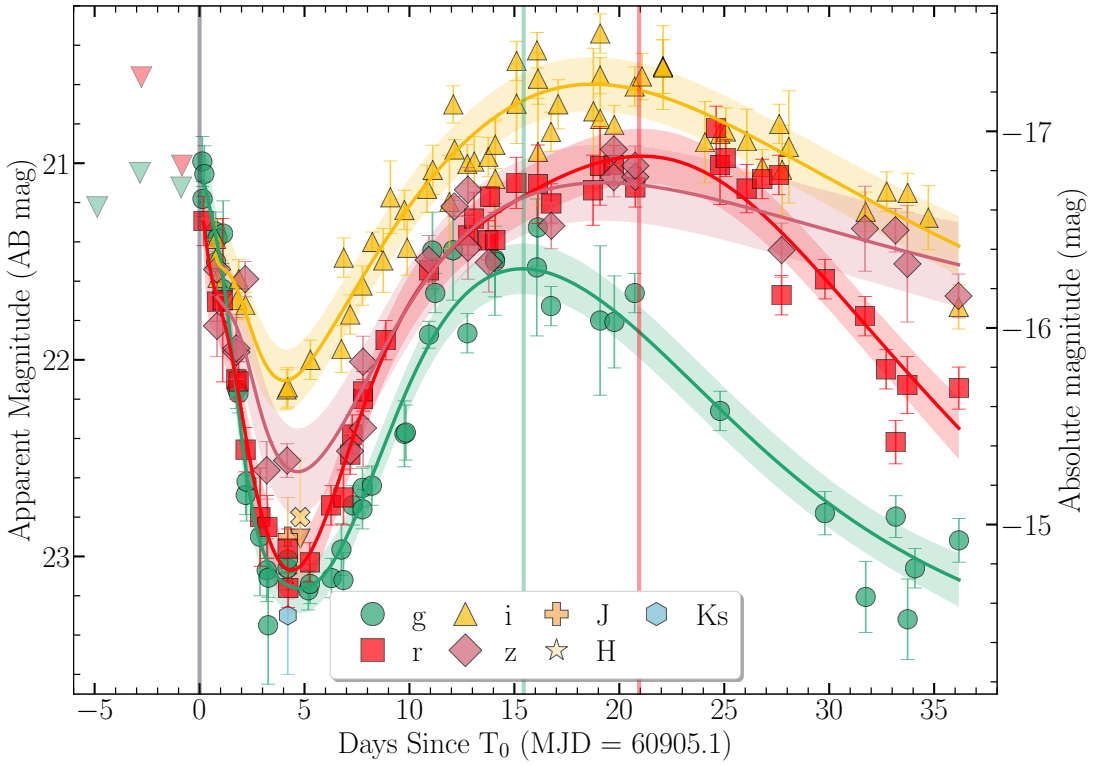

Figure 2. Optical and near-infrared light curve of ZTF 25abjmnps (AT2025ulz). The filters *g*, *r*, *i*, *z*, *J*, *H*, and *Ks* are shown with different colors and different symbols. We show with a vertical line the onset of S250818k, defined as $t = 0$ days, with other vertical lines for the second *g*-band peak and the second *r*-band peak. The GP fits to the light curves are shown with the solid colored lines and the uncertainties as the shaded regions.

comparison to SN templates, we normalized each spectrum and the template set to a common scale. The observed spectrum is first dereddened, and the narrow host lines and telluric bands are masked. A smooth continuum is then estimated using a cubic spline using *scipy*, iteratively reweighted with Tukey biweights implemented in *numpy*, following the standard bisquare form, which suppress the influence of strong lines and outliers, providing a stable approximation to the underlying spectral shape. The spectrum is divided by this continuum, and the resulting ratio is centered and rescaled by subtracting its median value and linearly mapping the central flux distribution to the ± 1 interval. This normalization emphasizes line morphology while minimizing sensitivity to absolute flux calibration (Section 5).

4. Is ZTF 25abjmnps a Kilonova?

In the first few days after discovery, the fast decline, the reddening of the color, and the featureless optical spectra of ZTF 25abjmnps were reminiscent of GW170817. A direct comparison to GW170817, as well as model fits to the light curve using a kilonova model grid, gave reasonable ejecta properties. When the light curve started to plateau and then rise, we explored the hypothesis that an off-axis afterglow-like relativistic component may be contributing to the emission. We find that joint kilonova and afterglow models can indeed fit the entire optical light curve, but the derived parameters are not consistent with the nondetections in the radio and X-ray.

First, we focus on the optical data in the first 2.5 days and fit these data with kilonova models. Specifically, we employ a grid of merging binary neutron star kilonova models computed with the Monte Carlo radiative transfer code POSSIS (M. Bulla 2019, 2023) and recently presented in T. Ahumada et al. (2025). Briefly, the grid is constructed by varying the mass, averaged velocity, and averaged electron fraction of two ejecta components (E. Nakar 2020)—a first axially symmetric high-velocity component ejected during the merger (dynamical ejecta) and a second spherically symmetric low-velocity component ejected from the post-merger disk (disk wind ejecta). When varying the six free parameters ($m_{\rm dyn}$, $\bar{v}_{\rm dyn}$, $\bar{Y}_{e\,\rm dyn}$, $m_{\rm wind}$, $\bar{v}_{\rm wind}$, and $\bar{Y}_{e\,\rm wind}$) within ranges predicted by numerical relativity simulations (D. Radice et al. 2018; V. Nedora et al. 2021), and accounting for 11 different viewing angles $\theta_{\rm obs}$, a total of 33,792 different kilonova models are fitted to the available photometry.

The best-fit kilonova model gave a good fit to the optical photometry data in the first 3 days (reduced $\chi^2 = 1.05$). The best-fit model corresponds to the following parameters: $m_{\rm dyn} = 0.02\,M_\odot$, $\bar{v}_{\rm dyn} = 0.2$c, $\bar{Y}_{e\,\rm dyn} = 0.2$, $m_{\rm wind} = 0.09\,M_\odot$, $\bar{v}_{\rm wind} = 0.03$c, $\bar{Y}_{e\,\rm wind} = 0.3$, and $\theta_{\rm obs} = 25.^\circ 8$. In particular, the relatively high masses inferred for both ejecta components are due to the relatively high luminosities of ZTF 25abjmnps, which is $\sim$0.5–1.0 mag brighter than GW170817 and peaks at an absolute magnitude of ~ -17 mag. An NMMA (P. T. H. Pang et al. 2023) fit to the early light curve is presented in a companion Letter (X. J. Hall et al. 2025a). The inferred viewing angle and the lack of high-energy detections (C. de Barra 2025) are suggestive of an off-axis event but not well constrained by the early data alone.

The peak time of an afterglow depends on the off-axis angle: the difference between the jet core angle and the viewing angle $\theta_c - \theta_{\rm obs}$. In the case of AT2017gfo, light-curve modeling and very long baseline interferometry measurements of the superluminal motion of its jet yielded a viewing angle of $\approx 19^\circ$, and the jet core angle was estimated to be $1.^\circ 5$–4°. The

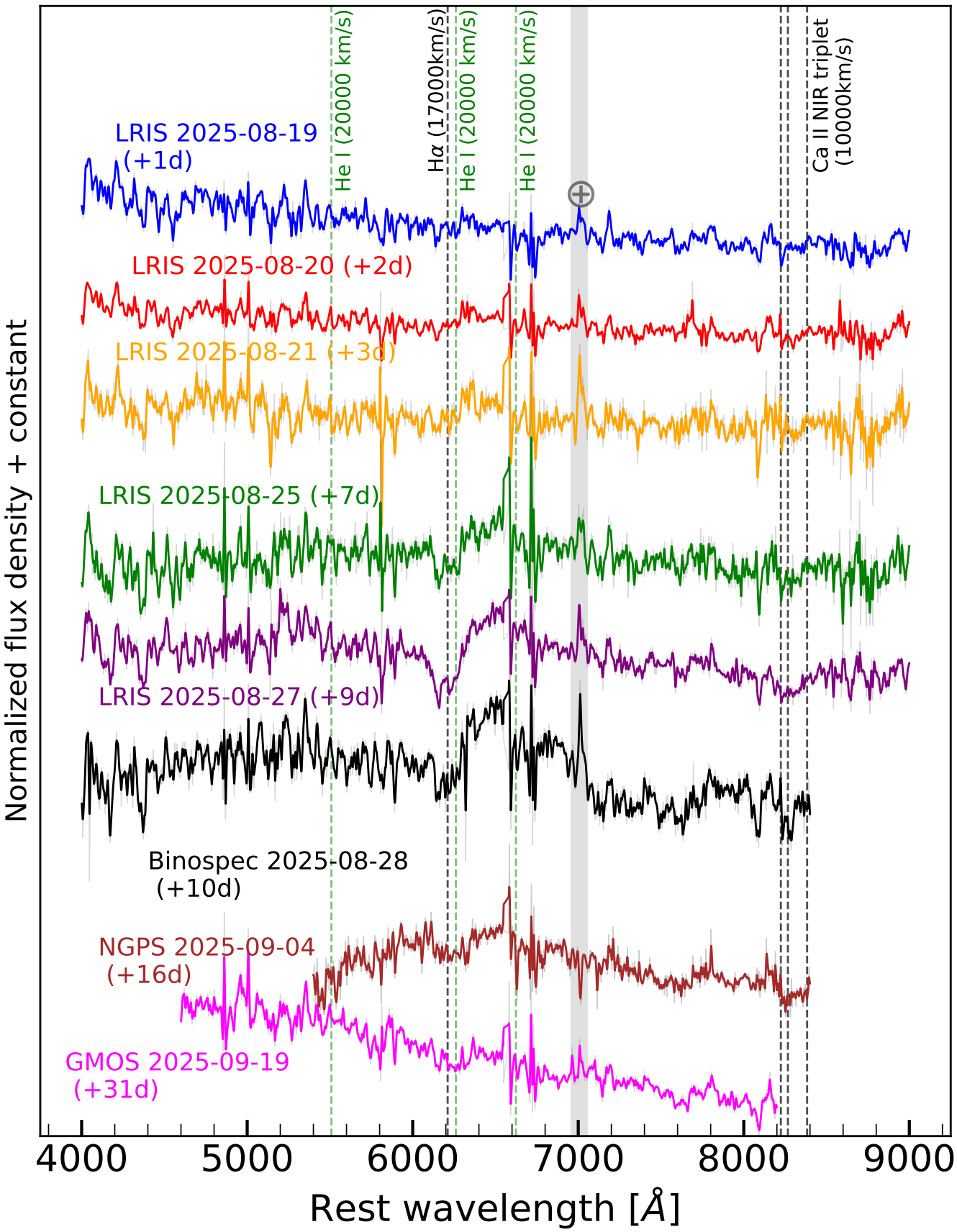

Figure 3. Spectroscopic evolution of ZTF 25abjmnps subtracting a scaled archival host spectrum (X. J. Hall 2025; X. J. Hall et al. 2025b). A blue featureless continuum evolved to become redder and then showed prominent broad P Cygni features. Hydrogen, helium, and calcium lines are marked with vertical dashed lines at the velocities indicated in parentheses. The spectral range impacted by telluric correction is shown with a gray shaded line and should be ignored. The flux calibration in the GMOS spectrum is impacted by using a flux calibrator on a different night instead of the same night.

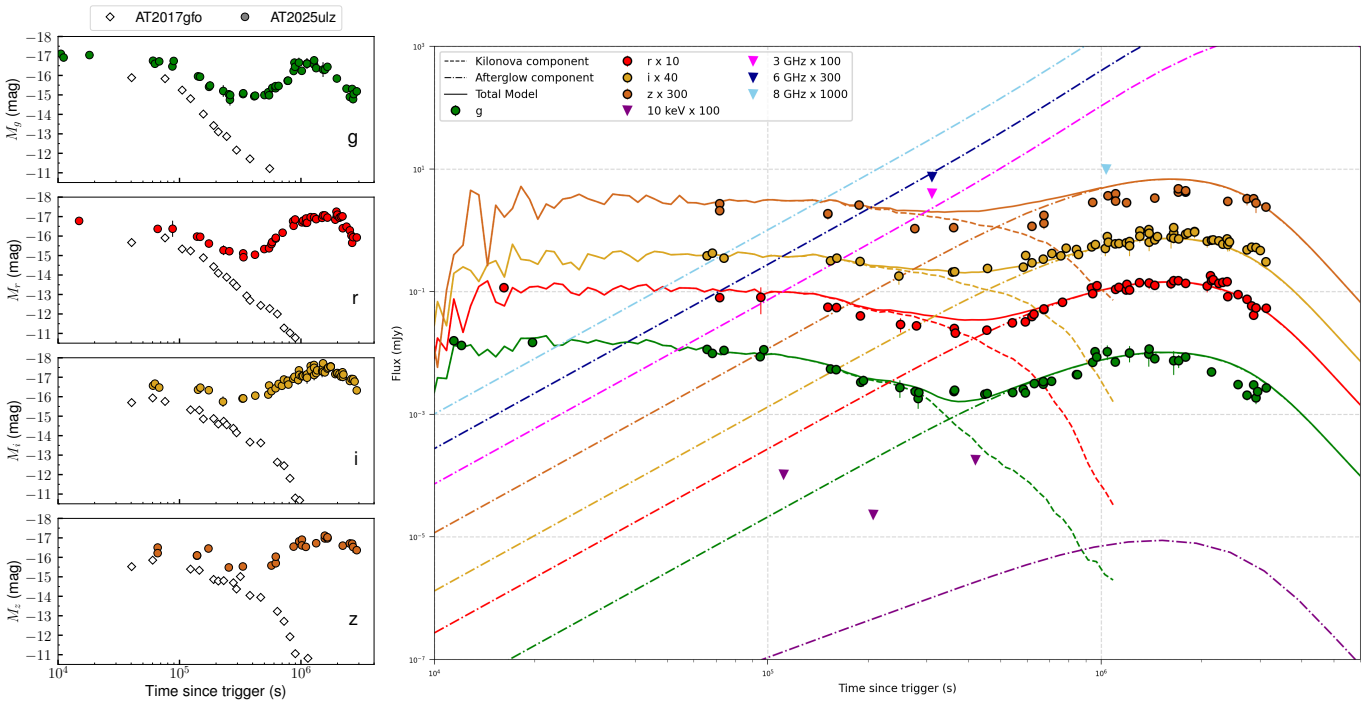

Figure 4. Left panels: griz light curves of ZTF 25abjmnps (filled circles) compared to GW170817/AT2017gfo (open diamonds). Right panel: Combined kilonova and off-axis afterglow model plotted with the observed data. The best-fit kilonova model corresponds to the following parameters: $m_{\rm dyn} = 0.02\,M_\odot$, $\bar{v}_{\rm dyn} = 0.2$c, $\bar{Y}_{e\,\rm dyn} = 0.2$, $m_{\rm wind} = 0.09\,M_\odot$, $\bar{v}_{\rm wind} = 0.03$c, $\bar{Y}_{e\,\rm wind} = 0.3$, and $\theta_{\rm obs} = 12^\circ$. The afterglow fit yields $\log_{10}(E_0/{\rm erg}) = 53.88 \pm 0.08$ with an external medium density of $\log_{10}(n_0/{\rm cm}^{-3}) = -0.97 \pm 0.09$. The structured jet has an initial Lorentz factor of 48.20 ± 15.11, with the jet core angle being $\theta_c = 1\overset{\circ}{.}42 \pm 0\overset{\circ}{.}12$ and the viewing angle being $\theta_{\rm obs} = 12\overset{\circ}{.}04 \pm 0\overset{\circ}{.}21$. The electron energy distribution is characterized by an index of $p = 2.88 \pm 0.08$. Note that for a better-constrained fit, we fixed the microphysical parameters to typical afterglow values, adopting $\epsilon_e = 0.1$ and $\epsilon_b = 0.01$.

large difference led to the afterglow light curve peaking about 150 days after the merger (K. P. Mooley et al. 2018, 2022; G. Ghirlanda et al. 2019; T. Govreen-Segal & E. Nakar 2023). We modeled the afterglow using JETSIMPY (H. Wang et al. 2024), which models the data as synchrotron emission from a structured jet that interacts with an external medium. We assume a structured jet with a Gaussian profile defined as

$$E(\theta) = E_{\rm K,iso} \quad exp\left[-\frac{1}{2}\left(\frac{\theta}{\theta_c}\right)^2\right], \tag{1}$$

$$\Gamma(\theta) = (\Gamma_0 - 1) \quad exp\left[-\frac{1}{2}\left(\frac{\theta}{\theta_c}\right)^2\right] + 1, \tag{2}$$

where $E_{\rm K,iso}$ is the isotropic equivalent energy, Γ_0 is the initial Lorentz factor, and θ_c is the jet half-opening angle.

We assume that the early data are dominated by the kilonova, with negligible contribution from the afterglow, and thus the kilonova model provides a good description of the early observations. Since the kilonova model fades rapidly after about 2×10^5 s, we leave a small gap and select data after 3×10^5 s as "afterglow-dominated," and perform a fit with JETSIMPY to calculate the jet parameters, following the procedures described in V. Swain et al. (2025). We find a smaller viewing angle so go back and redo the kilonova fit with additional POSSIS simulations with a finer grid resolution in terms of viewing angle. With this iterative joint fit, we find a best-fit model, as shown in Figure 4, with the best-fit parameters in the figure caption. We note that this is not the only solution—running joint fits using the NMMA framework (P. T. H. Pang et al. 2023) yields fits with lower energy.

Comparing to the afterglow modeling in B. O'Connor et al. 2025, the best-fit model here explores parameter space that is farther off-axis and of higher circumstellar density. However, while the best-fit model appears to roughly explain all the optical photometry, it is inconsistent with the deeper radio upper limits (B. O'Connor et al. 2025; A. Corsi et al. 2025, in preparation) and marginally inconsistent with the deeper X-ray observations (B. O'Connor et al. 2025) that are presented in companion Letters. Furthermore, the afterglow interpretation for ZTF 25abjmnps is also inconsistent with the detailed photometric color evolution and the P Cygni features observed in the optical spectra that we discuss next. Our conclusion that ZTF 25bjmnps is not a canonical GW170817-like kilonova is consistent with the independent analysis in multiple Letters (N. Franz et al. 2025; J. H. Gillanders et al. 2025; X. J. Hall et al. 2025a; B. O'Connor et al. 2025; Y.-H. Yang et al. 2025). The joint kilonova and afterglow fit result does underline the need to obtain spectroscopic follow-up, radio follow-up, and X-ray follow-up for future events and not rely on optical photometry alone.

5. Is ZTF 25abjmnps an SN?

With subsequent follow-up data, there were two major clues suggesting an SN origin to ZTF 25abjmnps. First, the appearance and strengthening of a P Cygni profile in the optical spectra, which, if showing Hα at 17,000 km s^{-1}, would indicate a core-collapse SN. Second, a luminous second peak reminiscent of stripped-envelope SNe, specifically Type IIb SNe, where the first peak is attributed to shock cooling and the second peak to the radioactive decay of ^{56}Ni. Our spectroscopic classification below of ZTF 25abjmnps as a Type IIb

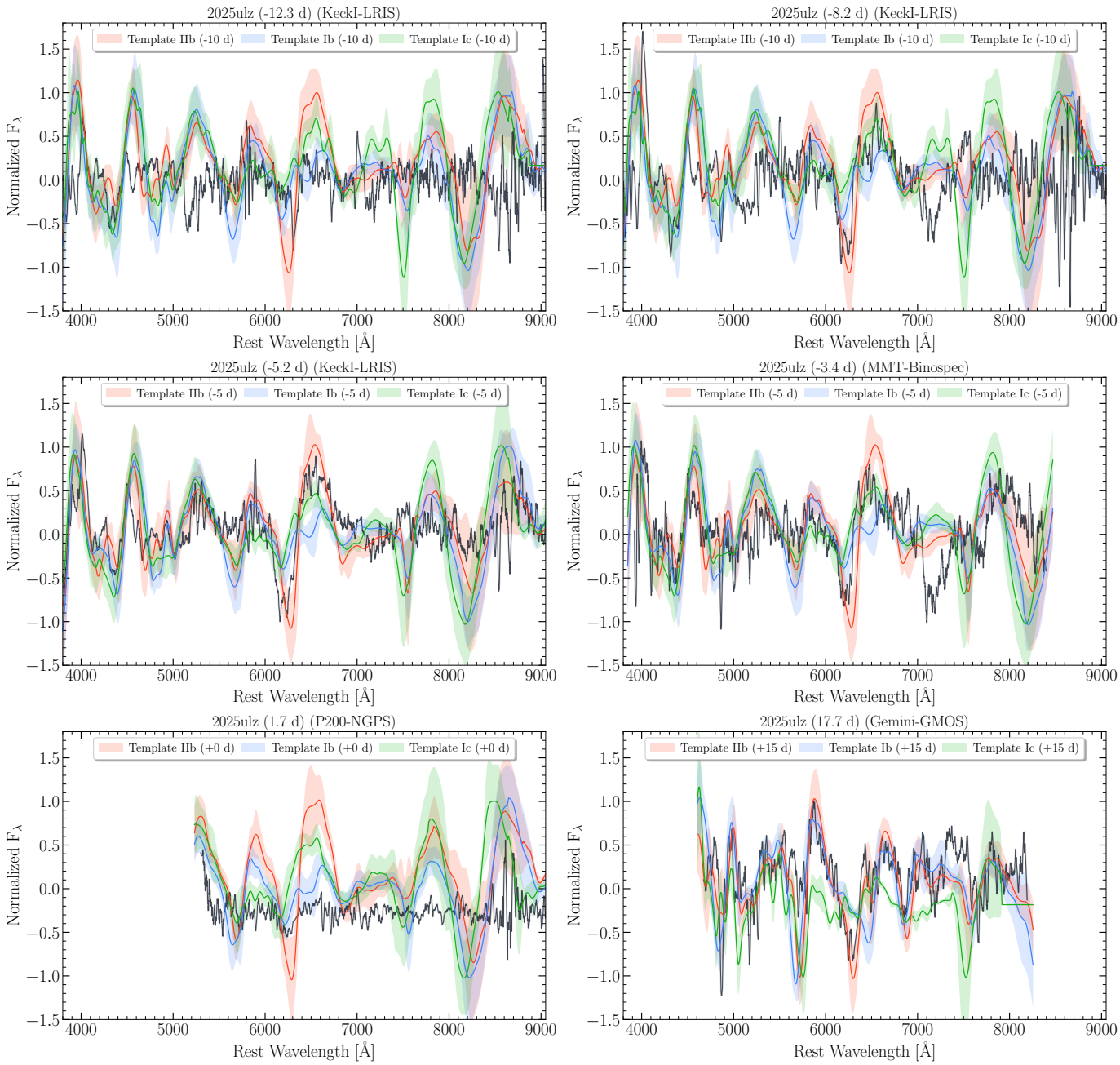

Figure 5. Comparing ZTF 25abjmnps with template spectra of SNe IIb, Ib, and Ic from Y.-Q. Liu et al. (2016) and M. Modjaz et al. (2016). The templates were constructed from phase-binned, flattened mean spectra, with the shaded regions representing 1σ diversity in each subclass. The observed spectra were extinction-corrected and continuum-subtracted after masking the telluric features and narrow host emission lines. The matches to Hα before maximum (panels (2), (3), and (4)) and helium after maximum (panel (6)) as well as the absence of O I support the spectroscopic classification as a Type IIb SN.

SN is consistent with the independent analysis presented in multiple Letters (N. Franz et al. 2025; J. H. Gillanders et al. 2025; X. J. Hall et al. 2025a; B. O'Connor et al. 2025; Y.-H. Yang et al. 2025). However, a Type IIb classification does not preclude association with S250818k. Thus, next, we compare ZTF 25abjmnps to a literature sample of well-studied stripped-envelope SNe (Type IIb, type Ib, and type Ic) to better understand the similarities and differences.

Spectroscopically, the first three observations (at +1, +2, and +3 days) show that the continuum gets redder, but they do not allow a classification, as they are featureless (Figure 3). The next three spectra (at +7, +9, and +10 days) show a strengthening of a P Cygni profile with an absorption minimum around 6200 Å, and the next two spectra (at +16 and +31 days) show a weakening of the same feature (Figure 3). We compare the normalized spectra with stripped-envelope SN templates (Y.-Q. Liu et al. 2016; M. Modjaz et al. 2016) in Figure 5. The relatively best match is to a Type IIb SN at −5 days from the second peak, with the putative P Cygni feature being Hα at 17,000 km s^{-1} (Figure 5). However, the strength of the same feature is weaker at other phases relative to the templates. We consider whether the putative P Cygni feature could be He I at 20,000 km s^{-1}, as in a type Ib SN, instead of Hα, but find that the absence of He I λ5876 (usually a stronger transition) is inconsistent with this interpretation. We also consider whether the putative P Cygni feature could

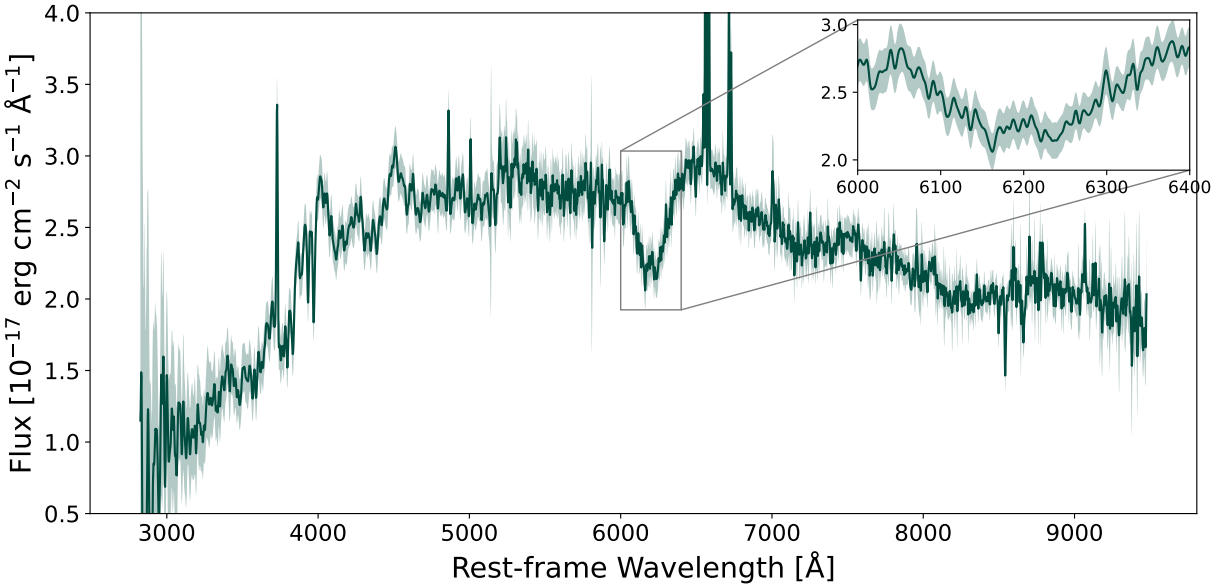

Figure 6. Spectrum before subtracting host light. Note the zoom-in on the P Cygni feature showing the W-shaped profile instead of a U-shaped profile.

be due to Si II at 8000 km s^{-1}, as in a type Ic SN. However, the absence of the O I λ7774 line suggests it is not a type Ic SN (I. Shivvers et al. 2019). The emergence of helium features, especially He I 5876, in the spectrum after second peak (+17.7 days) supports the Type IIb classification. We note a confounding detail—the shape of the putative Hα absorption feature was a "W shape" and not the usual "U shape," suggesting a doublet not a singlet line or a more complicated ejecta geometry (Figure 6). One possibility is that this line is a blend of Hα and He I at 20,000 km s^{-1}. If so, it is surprising that He I 5876 is not detected at this phase. If this was the Si II doublet, the separation between the absorption dips does not match to the same velocity. Overall, ZTF 25abjmnps is spectroscopically most consistent with being a stripped-envelope SN of Type IIb with some small oddities about line strength and line shape when compared to templates.

Photometrically, we compare the color evolution and light-curve evolution to a literature sample of Type IIb and type Ib SNe and some theoretical models that vary mixing (Figure 7). Similar to Type IIb SNe, ZTF 25abjmnps shows two peaks, albeit with a somewhat steeper evolution after the first peak. However, we find that the $r-i$ color evolution before the second peak and the $g-r$ color evolution after the second peak are unusual compared to other Type IIb SNe (Figure 7, bottom left panel and middle left panel). There are three possibilities for this unusual color evolution. First, we consider the extinction corrections (the solid line versus the dashed line in Figure 7) and find that even by using the upper limit on the dust from Section 3, we cannot explain the color. Second, we consider whether it could be a k-correction effect, as the literature sample is at significantly lower redshifts than ZTF 25abjmnps, and the most prominent P Cygni feature in the spectrum straddles the r and i bands. Quantifying this correction precisely is challenging, due to the host galaxy light contamination in the spectra. We roughly estimate that k-correction could explain up to 0.3 ± 0.1 mag of $r-i$ color at 5 days but not the full 0.9 mag deviation from the literature sample. Third, it is possible that the odd color evolution is due to opacity effects, such as hydrodynamic mixing by disk winds of a small quantity of heavy elements produced by the r-process (J. Barnes & P. C. Duffell 2023), or perhaps even some mixing of Fe-group elements (S.-C. Yoon et al. 2019). A detailed model for the mixing and opacity is outside the scope of this Letter.

Next, to understand the energetics, we fit a radiation hydrodynamics model to the light curve. To create an SN IIb progenitor model, we start with the models developed by G. Long et al. (2022) produced with the Modules for Experiments in Stellar Astrophysics (MESA) code (B. Paxton et al. 2011, 2013, 2015, 2018, 2019; A. S. Jermyn et al. 2023). We use the model with rotation from G. Long et al. (2022),[45] modified to initial masses between $17M_{\odot}$ and $15M_{\odot}$, and an orbital period of 300 days. The evolution of this system results in an SN-IIb-like progenitor with an envelope radius $R_{\rm env} \approx 450R_{\odot}$. We use the SuperNova Explosion Code (SNEC; V. Morozova et al. 2015) to explore a grid of pre-SN stellar models based on the binary model described above. This grid covers $E_{\rm kin} = 1.0$–1.8×10^{51} erg, $M_{^{56}\rm Ni}$ 0.08–0.18 $M_{\odot}$, $R_{\rm env}$ 100–200 $R_{\odot}$, and $M_{\rm ej}$ 3.0–3.8 $M_{\odot}$.[46] To achieve the range of different envelope radii, we modified the bound envelope radius of the original $R_{\rm env} = 450$ $R_{\odot}$ model by cutting the model grid appropriately before running SNEC. We exploded all models in the grid using a thermal bomb with ^{56}Ni mixed all the way through the remaining star after mass excision. We also allow for a shift ΔT with respect to T_0 of S250818k and a varying $E(B-V)$ during our fitting.

The resulting light curves were compared to ZTF 25abjmnps. We find that the optimal[47] explosion parameters for ZTF 25abjmnps within this grid are $R_{\rm env} \approx 140R_{\odot}$, $M_{\rm env} \sim 0.06M_{\odot}$, $M_{\rm ej} \sim 3.0M_{\odot}$, $M_{^{56}\rm Ni} \sim 0.1$ $M_{\odot}$, $\rm E_k = 1.6$foe, $\Delta T = -1.4$ days, and $E_{B-V} = 0.2$ mag. This MESA+SNEC model is shown in Figure 8. We cannot measure reliable photospheric expansion velocities from our spectral sequence (e.g., from Fe II), but the best-fitting model velocities were checked to not

[45] Available at doi:10.5281/zenodo.6578992: G. Long (2022).
[46] Achieved by modifying the mass excision between 1.2 and 2.0 $M_{\odot}$.
[47] Based on χ^2 fitting.

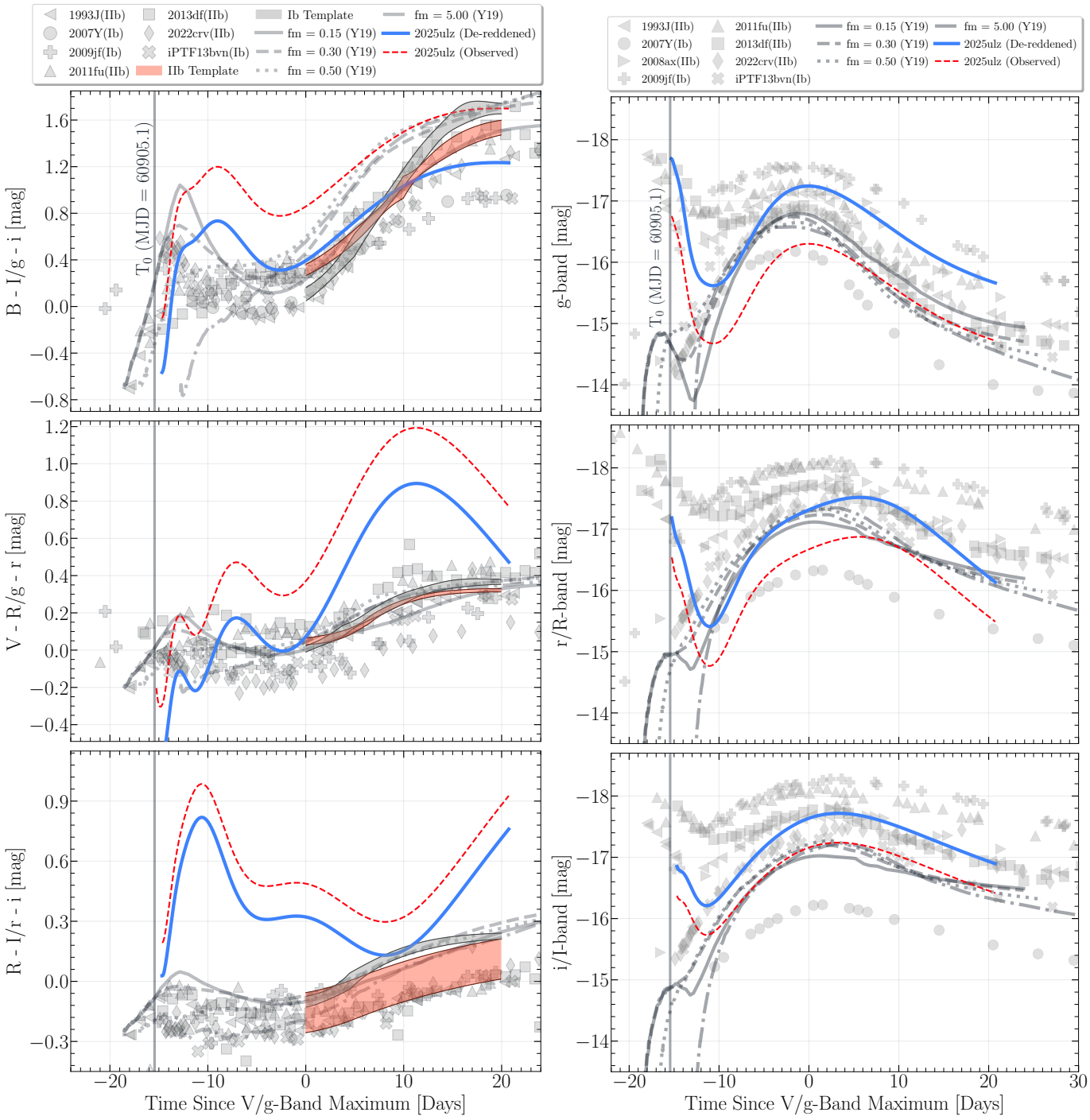

Figure 7. Left panels: comparing the color evolution of ZTF 25abjmnps with canonical Type IIb SNe and some templates (observed and dereddened curves are shown as dashed and solid lines, respectively). Also shown for comparison are synthetic color curves of SN Ib models by S.-C. Yoon et al. (2019), with varying degrees of ^{56}Ni mixing (higher fm is stronger ^{56}Ni mixing). Right panels: comparing the light curve of ZTF 25abjmnps to the same literature sample of well-studied Type IIb and type Ib SNe. Note the steeper decline of the *g*-band and *r*-band light curves.

be higher than the velocities measured from the Hα absorption minima.

We compare the explosion parameters to those of previously modeled SNe IIb (e.g., F. Taddia et al. 2018; N. Sravan et al. 2020). For example, SN 1993J had $M_{\rm ej} \sim 2.5$-$3.0 M_{\odot}$, $M_{^{56}\rm Ni} \sim 0.08$ $M_{\odot}$, Ek ~ 1.0–1.2 foe, and a progenitor radius of $\sim 600 R_{\odot}$ (K. Nomoto et al. 1993; S. E. Woosley et al. 1994). SN 2011dh was modeled with $M_{\rm ej} \sim 1.8$–$2.5 M_{\odot}$, $M_{^{56}\rm Ni} \sim 0.06$ $M_{\odot}$, Ek ~ 0.6-1.0 foe, and a progenitor radius of $\sim 200 R_{\odot}$ (M. C. Bersten et al. 2012; M. Ergon et al. 2014). Similarly, SN 2013df showed $M_{\rm ej} \sim 2.0$–$3.5 M_{\odot}$, $M_{^{56}\rm Ni} \sim 0.1$ $M_{\odot}$, Ek ~ 0.8–1.2 foe, and a progenitor radius of $\sim 550 R_{\odot}$ (A. Morales-Garoffolo et al. 2014). Thus, ZTF 25abjmnps falls within the canonical Type IIb SN parameter space, except for an apparently smaller envelope radius and somewhat higher kinetic energy, though there may be a selection bias against small radii, since their durations are fast and rarely well enough sampled for detailed modeling. Based on

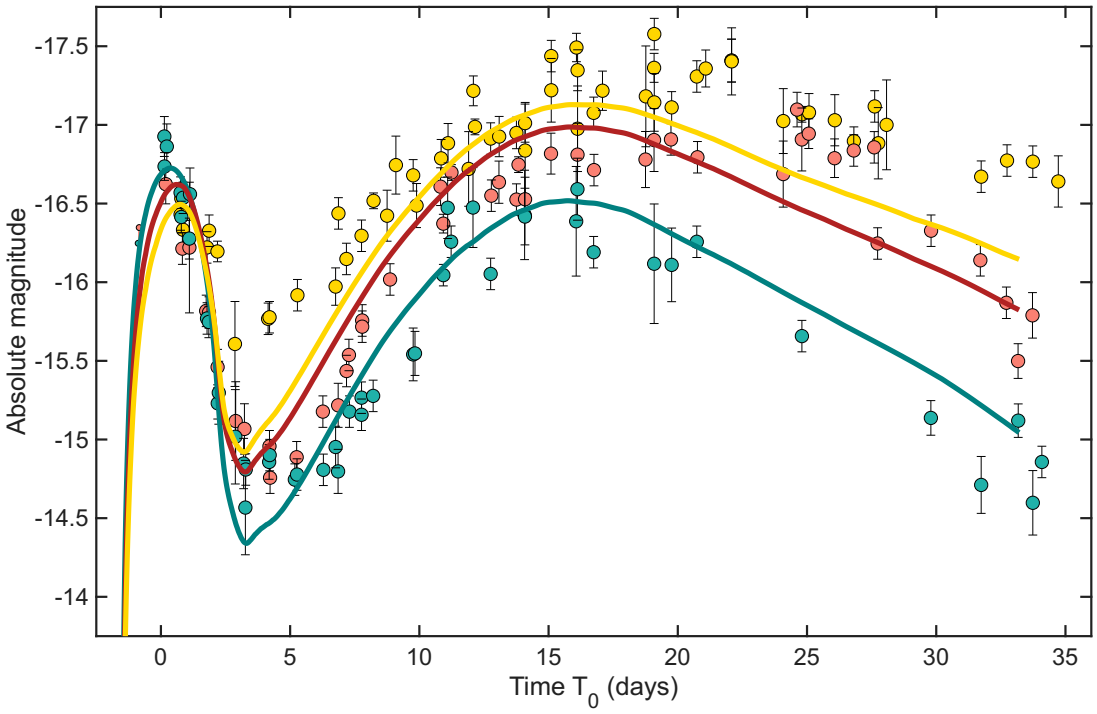

Figure 8. Hydrodynamic model fit to ZTF 25abjmnps using an SN IIb progenitor model with an extended envelope radius $R_{\rm env} \approx 140 R_{\odot}$, $M_{\rm ej} \sim 3.0 M_{\odot}$, $M_{\rm env} \sim 0.06 M_{\odot}$, $M_{^{56}\rm Ni} \sim 0.1 M_{\odot}$, $E_k = 1.6$foe, $\Delta \rm T = -1.4$ days, and $E_{B-V} = 0.2$mag. Note the colors are g band (green), r band (red), and i band (yellow). The pre-explosion upper limit used in the fit is at 3σ.

the derived parameters, ZTF 25abjmnps is more likely to have a binary progenitor.

Finally, to estimate the chance coincidence of discovering a young Type IIb SN in the observed snapshot GW volume within 1 day of explosion, we do the following back-of-the-envelope calculation: $1 - \exp(-\rm Volume^{*}Age^{*}Rate)$. To estimate the volume, we consider a spherical shell between 150 Mpc and 400 Mpc (corresponding to the GW constraints) and a fractional all-sky volume of 0.008962 (corresponding to the 369.7 deg^2 searched) and get 2.276×10^6 Mpc^3. For age, we assume the transient is within one day of explosion, so a time window of 1/365 yr. For the rate of Type IIb SNe, there is an unresolved discrepancy between magnitude-limited survey estimates and volume-limited survey estimates. We assume a Type IIb fraction of 12%, relative to the type II SNe from W. Li et al. (2011) and the type II rate from K. K. Das et al. (2025) of 3.9×10^{-5} Mpc^{-3} yr^{-1}. Thus, our net chance coincidence estimate is crudely 2.9%. A more recent estimate of the Type IIb volumetric rate by ASAS-SN was $0.8^{+0.6}_{-0.4} \times 10^{-5}$ Mpc^{-3} yr^{-1} (T. Pessi et al. 2025)—this gives a chance coincidence rate of $4.9^{+3.5}_{-2.5}$%. We caution that this is not a robust estimate, for many reasons: we have not folded in the joint significance of the EM and GW, trials factors, the detection efficiency of ZTF, or the fraction of Type IIb SNe that show the peculiar properties of ZTF 25abjmnps. While a more detailed estimate is beyond the scope of this Letter, as it awaits the offline GW analysis, this back-of-the-envelope estimate tells us that the chance coincidence of finding a young stripped-envelope SN in the GW localization is not negligible. As described in Appendix B, we further reanalyze our candidate vetting procedure to thoroughly check if there may be any other young stripped-envelope SN that may be coincident with S250818k, and ZTF 25abjmnps remains the most compelling candidate.

6. Discussion: Are ZTF 25abjmnps and S250818k Related by a Superkilonova Model?

To summarize, ZTF 25abjmnps is an optical transient that is spatially and temporally coincident with the GW signal. While the optical light curve fits a kilonova and afterglow model, the optical spectral features and radio/X-ray upper limits are inconsistent with this picture. While the optical spectra and light curves are most similar to those of a Type IIb SN, there are some differences in the color evolution and spectral feature strength/shape when compared to the literature sample of Type IIb SNe. The key GW clue is that this may represent the merger of neutron stars lighter than a solar mass. Next, we explore a potential tantalizing multimessenger association in the context of a superkilonova model.

In principle, stable neutron stars can exist and be as small as 0.1 $M_{\odot}$ (e.g., P. Haensel et al. 2002). However, the formation of a subsolar neutron star presents a major challenge to stellar evolution. Detailed modern simulations of the core collapse and SN explosion of (slowly spinning) massive stars predict a robust lower limit to the neutron star mass of 1.2 $M_{\odot}$, similar to the Chandrasekhar mass of the progenitor's iron core (B. Müller et al. 2025). A similar lower limit applies to the masses of neutron stars formed from the accretion-induced collapse of a white dwarf (e.g., K. Nomoto & Y. Kondo 1991). The only solution to forming a subsolar-mass neutron star is to identify a neutron-rich environment, as the Chandrasekhar mass is proportional to the square of the electron fraction. One such gravitating neutron-rich environment is possible in the immediate aftermath of the collapse of a rapidly spinning star. It has been proposed that collapsing stars may undergo fission

of the collapsing core into two neutron stars instead of one (R. H. Durisen & J. E. Tohline 1985; V. S. Imshennik & D. V. Popov 1998; M. B. Davies et al. 2002; K. A. Postnov et al. 2016), although this has yet to be demonstrated with detailed numerical simulations. Separately, it has also been proposed that if the stellar envelope has sufficient angular momentum, then rather than accreting directly onto the central compact object, it would initially form a centrifugally supported disk of material.

A sufficiently massive and large disk can become gravitationally unstable (A. Toomre 1964) and undergo fragmentation and collapse to form neutron stars, as a result of runaway neutrino cooling or alpha-particle dissociation (A. L. Piro & E. Pfahl 2007; B. D. Metzger et al. 2024; Y. Lerner et al. 2025). This process is qualitatively similar to the proposed mechanism for forming planets in protoplanetary disks (C. F. Gammie 2001) or stars in the disks of AGNs (J. Goodman & J. C. Tan 2004). Furthermore, if the disk becomes neutron-rich, as a result of electron captures on protons, then the lower Chandrasekhar mass limit could enable the formation of subsolar-mass neutron stars (B. D. Metzger et al. 2024). This was recently illustrated explicitly using shearing-box hydrodynamic simulations by Y.-X. Chen & B. D. Metzger (2025), who found that fragmentation into a spectrum of objects of mass ≈ 0.01–$1\ M_{\odot}$ is achieved for disks with high accretion rates. If the disk fragments into multiple neutron stars, these bodies may become paired into tight binaries, either as a result of fissioning from a single collapsing clump (e.g., D. Nesvorný et al. 2010) or through gas drag friction (e.g., M. Dodici & S. Tremaine 2024). The subsequent coalescence of these binaries, possibly after a delay of minutes to hours after the collapse, offers a potential source of GW emission in near coincidence with the SN (B. D. Metzger et al. 2024). Alternatively, if the disk fragments into a single subsolar neutron star, it will merge with the central (ordinary-mass) neutron star or low-mass black hole created by the core collapse, creating a single GW signal.

We posit that this idea of fragmentation in a collapsing core's accretion disk can qualitatively explain a possible multimessenger association between S250818k and ZTF 25abjmnps. First, the low chirp mass of S250818k leaves open the possibility that we are seeing the merger of one or two subsolar neutron stars, either with themselves or with the central compact object left over from the explosion. More details of the masses of the two components and revised FAR with an offline analysis of the GW strain will need to await future publication by the LIGO–Virgo–KAGRA collaboration. Second, the similarity of ZTF 25abjmnps to stripped-envelope SNe suggests that the progenitor star might have interacted with a binary, leaving it with enough angular momentum to form such an accretion disk that can fragment upon collapse. Although past work has focused on this possibility in the context of collapsars, there is no fundamental reason that rapid rotation and the associated disk formation are limited to the collapse of completely stripped stars or broadline type Ic SNe in particular. Indeed, the mechanisms for spinning up the cores of massive stars at late stages of evolution may be diverse (e.g., M. Cantiello et al. 2007; D. Tsuna et al. 2025) and in some cases may occur for progenitors with moderate amounts of hydrogen and helium. For example, a stellar merger that occurs soon before core collapse could both spin up the core and give rise to a type-IIb-like SN (e.g., S.-C. Yoon et al. 2017; N. Lohev et al. 2019). Third, the unusual color evolution may be indicative of a small amount of *r*-process elements getting mixed and contributing to the opacity for some time, until the nickel dominates (D. Kasen et al. 2013; J. Barnes & P. C. Duffell 2023). Fourth, the actively star-forming local environment of the host galaxy of ZTF 25abjmnps is a suitable location for such core-collapse events.

Establishing a firmer association between S250818k and ZTF 25abjmnps requires more detailed theoretical modeling and sensitive late-time observations. Late-time monitoring of the light curve could be compared to what is expected from heating by nickel-56. Nebular spectroscopy in the infrared (especially with the James Webb Space Telescope) would directly constrain the ejecta composition. Perhaps the high density of the surrounding medium in actively star-forming regions could aid radio detections at late time. Additional radio and X-ray data would constrain whether or not there is a late-time relativistic nonthermal component. If the accretion disk or disk-embedded merger events power relativistic jets, this could impart asymmetry to the SN explosion along the rotation axis and create a nonthermal afterglow if the jet can break through the envelope of the star. On the other hand, a larger envelope could stifle any accretion-powered jet, rendering signatures of the central engine less apparent than in traditional GRBs. While late-time radio/X-ray detections would support this idea, late-time radio/X-ray nondetections would not rule out this superkilonova model. Perhaps the most vivid proof of such a superkilonova model would be if the GW signature itself showed signs of multiple mergers—for example, a subsolar neutron star merger followed by a neutron star–black hole merger. A neutron star–black hole merger is only expected in the superkilonova picture if the accretion disk fragmented to form the subsolar neutron stars. It is not expected in the superkilonova picture if the collapsing core directly fissioned into two neutron stars that merged or if the fragmentation formed only one subsolar neutron star that merged with a central neutron star.

Looking back to previous multimessenger searches of neutron star mergers, stripped-envelope SNe have been rejected as associated at least twice. First, DG19wxnjc (AT2019npv) was a type-Ib-like SN that was spatially and temporally coincident with the neutron star–black hole merger GW190814 (I. Andreoni et al. 2020). However, the age of the SN was unconstrained in this case, and the gravitational event could have been a binary black hole merger. Second, AT2019wxt was an ultrastripped SN that was rejected during follow-up of S191213g (I. Agudo et al. 2023; H. Shivkumar et al. 2023). However, the astrophysical significance of the GW data was deemed questionable. More generally, a reexamination of past subthreshold events may be warranted in the context of the superkilonova model.

Looking ahead, there are many ways to test whether or not this potential multimessenger association between S250818k and ZTF 25abjmnps is correct. With future more sensitive GW interferometers in O5 and beyond, there should be many more detections of subsolar binary neutron star mergers at higher significance and better localization. Looking for an associated stripped-envelope core-collapse SN-like signature would be straightforward even to farther distances with the next generation of surveyors: e.g., the Vera C. Rubin Observatory (Ž. Ivezić et al. 2019; I. Andreoni et al. 2022), the Roman Space Telescope (I. Andreoni et al. 2024), DSA-2000 (G. Hallinan et al. 2019; D. Dobie et al. 2021), the UVEX

satellite (S. R. Kulkarni et al. 2021; A. W. Criswell et al. 2025), and the Cryoscope in Antarctica (M. M. Kasliwal et al. 2025). Any transient that looks like a young, stripped-envelope SN coincident with a subsolar neutron star merger or a neutron star–black hole merger should be followed up extensively at all wavelengths. More detailed theoretical modeling of a superkilonova, especially light-curve and spectra predictions, would help the observers optimize their follow-up observations. Continuing to have information such as the binned chirp mass and HasSSM in low latency is an important step toward multimessenger cooperation and would sharpen the telescope response. We remind the reader that all the optical photometry of ZTF 25abjmnps appears consistent with a canonical kilonova and afterglow model—spectroscopy, infrared, radio, and X-ray data are essential for ruling out this scenario. We caution against a rushed conclusion and encourage collecting and analyzing the full panchromatic dataset necessary to more firmly establish a multimessenger association.

In summary, we encourage the community to approach the future of multimessenger astrophysics with a wide-open view to new possibilities. When GW170817 happened in our backyard, the evidence for the multimessenger association was vivid, as the distinction between a kilonova and an SN was vast. Future multimessenger events may not look like GW170817, will likely be much farther away than GW170817, and may even show similarities to SNe. Nevertheless, there is an opportunity here to discern a "veritable multimessenger symphony" (B. D. Metzger et al. 2024) of a superkilonova—a core-collapse SN, a neutron star merger, and even a neutron star–black hole merger at the same time.

Acknowledgments

The authors thank the anonymous referee for the thoughtful feedback. M.M.K. thanks E. Nakar and K. Hotokezaka for valuable real-time brainstorming discussions. Mahalo to the W. M. Keck Observatory staff, especially M. Lundquist and J. O'Meara, and many observers for their full cooperation with multiple Target of Opportunity interruptions. M.M.K. thanks the participants of the ZTF Theory Network meeting at Oak Creek, especially Sterl Phinney, Eliot Quataert, Lars Bildsten, Daniel Brethauer, Wynn Jacobson-Galan, and Ryan Chornock, for many stimulating discussions, and this research has benefited from interactions supported by the Gordon and Betty Moore Foundation through grant GBMF5076.

A.S. acknowledges support from the Knut and Alice Wallenberg Foundation through the "Gravity Meets Light" project. B.D.M. acknowledges partial support from the National Science Foundation (grant AST-2406637) and the Simons Foundation (grant 727700). The Flatiron Institute is supported by the Simons Foundation. D.K. is supported in part by the U.S. Department of Energy, Office of Science, Office of Nuclear Physics, DE-AC02-05CH11231, DE-SC0004658, and DE-SC0024388, and by a grant from the Simons Foundation (622817DK). B.O. is supported by the McWilliams Postdoctoral Fellowship in the McWilliams Center for Cosmology and Astrophysics at Carnegie Mellon University. A.P., T.C., and L.H. are supported by NSF grant No. 2308193. M.B. acknowledges the Department of Physics and Earth Science of the University of Ferrara for the financial support through the FIRD 2024 grant.

Based on observations obtained with the 48 inch Samuel Oschin Telescope and the 60 inch Telescope at the Palomar Observatory as part of the Zwicky Transient Facility project. ZTF is supported by the National Science Foundation under grants No. AST-1440341, AST-2034437, and currently award #2407588. ZTF receives additional funding from the ZTF partnership. Current members include Caltech, USA; Caltech/IPAC, USA; University of Maryland, USA; University of California, Berkeley, USA; University of Wisconsin at Milwaukee, USA; Cornell University, USA; Drexel University, USA; University of North Carolina at Chapel Hill, USA; Institute of Science and Technology, Austria; National Central University, Taiwan; and OKC, University of Stockholm, Sweden. Operations are conducted by Caltech's Optical Observatory (COO), Caltech/IPAC, and the University of Washington at Seattle, USA. SED Machine is based upon work supported by the National Science Foundation under grant No. 1106171. The ZTF forced-photometry service was funded under the Heising–Simons Foundation grant #12540303 (PI: Graham). The Gordon and Betty Moore Foundation, through both the Data-Driven Investigator Program and a dedicated grant, provided critical funding for SkyPortal.

Some of the data presented herein were obtained at the Keck Observatory, which is a private 501(c)3 nonprofit organization operated as a scientific partnership among the California Institute of Technology, the University of California, and the National Aeronautics and Space Administration. The Observatory was made possible by the generous financial support of the W. M. Keck Foundation.

The 2 m HCT is located at the Indian Optical Observatory (IAO) at Hanle. We thank the staff of IAO, Hanle and CREST, Hosakote who made these observations possible. HCT observations were carried out under the ToO program of proposal number HCT-2025-C3-P43. The facilities at IAO and CREST are operated by the Indian Institute of Astrophysics, Bangalore.

This Letter includes observations made by the Two-meter Twin Telescope (TTT) sited at the Teide Observatory of the Instituto de Astrofísica de Canarias (IAC) that Light Bridges operates on the island of Tenerife, Canary Islands (Spain). The Observing Time Rights (DTO) used for this research were provided by Light Bridges, SL.

Based on observations at the Cerro Tololo Inter-American Observatory, NSF's NOIRLab (NOIRLab Prop. ID: 2025A-729671; PI: Palmese), which is managed by the Association of Universities for Research in Astronomy (AURA) under a cooperative agreement with the National Science Foundation. Based on observations obtained at the international Gemini Observatory, a program of NSF's NOIRLab, which is managed by the Association of Universities for Research in Astronomy (AURA) under a cooperative agreement with the National Science Foundation on behalf of the Gemini Observatory partnership: the National Science Foundation (United States), National Research Council (Canada), Agencia Nacional de Investigación y Desarrollo (Chile), Ministerio de Ciencia, Tecnología e Innovación (Argentina), Ministério da Ciência, Tecnologia, Inovações e Comunicações (Brazil), and the Korea Astronomy and Space Science Institute (Republic of Korea). The data were acquired through the Gemini Observatory Archive at NSF NOIRLab and processed using DRAGONS (Data Reduction for Astronomy from Gemini Observatory North and South). The authors wish to recognize and acknowledge the very significant cultural role and

reverence that the summit of Maunakea has always had within the indigenous Hawaiian community.

This Letter contains data obtained at the Wendelstein Observatory of the Ludwig-Maximilians University Munich. We thank Christoph Ries, Michael Schmidt, and Silona Wilke for performing the observations. Funded in part by the Deutsche Forschungsgemeinschaft (DFG, German Research Foundation) under Germany's Excellence Strategy—EXC-2094—390783311.

MMT Observatory access was supported by Northwestern University and the Center for Interdisciplinary Exploration and Research in Astrophysics (CIERA). C.L. and A.A.M. are supported by DoE award # DE-SC0025599, while A.A.M. is also supported by Cottrell Scholar Award # CS-CSA-2025-059 from the Research Corporation for Science Advancement. N.R. is supported by NSF award # 2421845.

The Liverpool Telescope is operated on the island of La Palma by Liverpool John Moores University in the Spanish Observatorio del Roque de los Muchachos of the Instituto de Astrofisica de Canarias with financial support from the UK Science and Technology Facilities Council.

This research used data obtained with the Dark Energy Spectroscopic Instrument (DESI). DESI construction and operations are managed by the Lawrence Berkeley National Laboratory. This material is based upon work supported by the U.S. Department of Energy, Office of Science, Office of High-Energy Physics, under Contract No. DE-AC02-05CH11231, and by the National Energy Research Scientific Computing Center, a DOE Office of Science User Facility, under the same contract. Additional support for DESI was provided by the U.S. National Science Foundation (NSF), Division of Astronomical Sciences, under Contract No. AST-0950945 to the NSF's National Optical–Infrared Astronomy Research Laboratory; the Science and Technology Facilities Council of the United Kingdom; the Gordon and Betty Moore Foundation; the Heising–Simons Foundation; the French Alternative Energies and Atomic Energy Commission (CEA); the National Council of Humanities, Science and Technology of Mexico (CONAHCYT); the Ministry of Science and Innovation of Spain (MICINN), and the DESI Member Institutions: www.desi.lbl.gov/collaborating-institutions. The DESI collaboration is honored to be permitted to conduct scientific research on I'oligam Du'ag (Kitt Peak), a mountain with particular significance to the Tohono O'odham Nation. Any opinions, findings, and conclusions or recommendations expressed in this material are those of the author(s) and do not necessarily reflect the views of the U.S. National Science Foundation, the U.S. Department of Energy, or any of the listed funding agencies.

CFH is part of a project that has received funding from the European Union's Horizon Europe Research and innovation program under Grant Agreement No 101131928. This project is based on observations obtained with MegaPrime/MegaCam, a joint project of CFHT and CEA/DAPNIA, at the Canada-France-Hawai'i Telescope (CFHT) which is operated by the National Research Council (NRC) of Canada, the Institut National des Sciences de l'Univers of the Centre National de la Recherche Scientifique (CNRS) of France, and the University of Hawai'i.

Appendix A
More Information about Follow-up Telescopes

FTW. We observed with the Three Channel Imager (3KK; F. Lang-Bardl et al. 2016) instrument mounted on the FTW (U. Hopp et al. 2014) in the g', r', i', z', and J bands. The optical CCD and near-infrared CMOS data were reduced using a custom pipeline developed at Wendelstein observatory (C. A. Gössl & A. Riffeser 2002; M. Busmann et al. 2025). For the astrometric calibration of the images, we used the Gaia EDR3 catalog (Gaia Collaboration 2020; Gaia Collaboration et al. 2021; L. Lindegren et al. 2021). We used the PS1 catalog (N. Kaiser et al. 2010) for the optical photometric calibration, and the Two Micron All Sky Survey (2MASS) catalog (M. F. Skrutskie et al. 2006) for the J band. Tools from the AstrOmatic software suite (E. Bertin & S. Arnouts 1996; E. Bertin et al. 2002; E. Bertin 2006) were used for the coaddition of each epoch's individual exposures. We used the Saccadic Fast Fourier Transform (SFFT; L. Hu et al. 2022) algorithm for image subtraction. For subtraction templates, we used Legacy Survey DR10 images (A. Dey et al. 2019) for the g, r, and z bands and PS1 imaging for the i band (N. Kaiser et al. 2010). FTW was able to provide a quick follow-up within hours of discovery, with two epochs showing a clear reddening and decline of the transient (see X. J. Hall et al. 2025a).

TTT. The TTT (M. Serra-Ricart et al. 2024), sited at the Teide Observatory of the Instituto de Astrofísica de Canarias, started observations 2.9 days post T_0 of ZTF 25abjmnps in the g, r, i, and z bands. We detected the transient in g, r, and i and obtained upper limits in z. We used the STDPipe pipeline and its web interface to perform forced photometry and template subtraction (S. Karpov 2025). For calibration, we used the PS1 catalog (K. C. Chambers et al. 2016). For the subtraction templates, we used Legacy Survey DR10 images (A. Dey et al. 2019) for the g and z images, PS1 for images in the i band, and MegaCam from the UNIONS survey[48] for the r band. We performed the subtraction using HOTPANTS (A. Becker 2015), with the convolution kernel size adjusted for every image individually, based on the FWHMs of the image and template.

CFHT/MegaCam. We acquired data using the MegaPrime camera mounted on the CFHT, in the g, r, i, and z bands, from 2025 August 21 to August 29. Similar to TTT, we used the STDPipe pipeline and its web interface to perform forced photometry and template subtraction (S. Karpov 2025).

LT. The robotic 2 m LT (I. A. Steele et al. 2004) observed the location of the transient on several occasions using the IO:O optical imager in the g, r, i, and z bands. Images were automatically processed by the LT data pipeline, and images were subtracted using PS1 imaging as a template. Point-spread-function (PSF) photometry is performed on the subtracted images.

SEDM. Mounted on the 60 inch Telescope at Palomar Observatory, the SEDM (N. Blagorodnova et al. 2018) took images in the g, r, and i bands throughout the duration of our campaign. Standard reduction techniques were applied to the data, and image subtraction revealed a clear excess at the location of the transient in multiple epochs.

WIRC. We acquired J- and Ks-band images with WIRC, mounted on the 200 inch Hale Telescope at Palomar Observatory. We performed standard calibrations, subtracted a UKIRT template to the images in the J band, and used the 2MASS (M. F. Skrutskie et al. 2006) catalog to calibrate the photometry.

MOSFIRE. We used MOSFIRE (I. S. McLean et al. 2012), mounted in the Keck II telescope, to observe ZTF 25abjmnps in the Y, J, H, and Ks bands. We used `mirar` to reduce the images and the PS1 and 2MASS catalogs for photometric calibration. When available, we performed image subtraction against the Hubble Space Telescope image. Otherwise, we used

[48] https://www.skysurvey.cc/releases/

galfit (C. Y. Peng et al. 2002) to model the galaxy, with an exponential and Sérsic profile to subtract the galaxy light.

Apache Point Observatory (APO). We observed with NICFPS (F. R. Hearty et al. 2004) mounted on the ARC 3.5 m telescope at Apache Point Observatory. We obtained dithered exposures in the *Z*, *J*, *H*, and *Ks* bands. We subtracted dark frames and constructed sky flats using custom Python routines (B. Bolin 2025, private communication) adapted from K. L. Weisenburger et al. (2017) and coadded the resulting images with SWarp (E. Bertin et al. 2002).

LRIS. We used LRIS (J. B. Oke et al. 1995), mounted in the Keck I telescope, to acquire *g*- and *I*-band photometry of ZTF 25abjmnps. Observations started with a 30 s sequence, followed by a 300 s exposure. We used lpipe (D. A. Perley 2019) to reduce the images, and we photometrically calibrated the images against PS1.

MMT. We collected optical photometry and spectroscopy with Binospec (D. Fabricant et al. 2019) mounted on the 6.5 m MMT telescope at the Fred Lawrence Whipple Observatory. Photometric observations were taken with the *r*, *i*, and *z* bands and reduced with the POTPyRI pipeline.[49] The astrometry is calibrated using Gaia DR3 astrometric standard stars, and the flux measurements are calibrated against PS1. We realized the subtraction on the images from the galaxy similar to the TTT and CFHT data analysis. Spectroscopic observations were taken with the 270-lines-per-millimeter grating, achieving $R \sim 1340$ with coverage between 3820 and 9210 Å. The spectroscopic reductions use pypeit (J. Prochaska et al. 2020) to automatically execute standard reduction procedures.

GMOS. With GMOS, mounted on the Gemini North telescope, we took slit spectrography on 2025 September 19 and imaged the location of ZTF 25abjmnps over six epochs between 2025 August 20 and 2025 September 31 in the *g*, *r*, *i*, and *z* bands (PI: Palmese; PI: O'Connor). The images were reduced with the DRAGONS pipeline (K. Labrie et al. 2019), and difference imaging was conducted with SFFT (L. Hu et al. 2022). Aperture photometry was conducted on the difference images using PS1 to calculate magnitude zero-points. The spectra were reduced with pypeit, with telluric corrections done through atmospheric modeling (J. Prochaska et al. 2020). More details are available in X. J. Hall et al. (2025a).

Blanco. We observed with the Dark Energy Camera (DECam) instrument mounted on the Blanco 4 m Telescope at the Cerro Tololo Inter-American Observatory using the *g*, *r*, and *z* bands (PI: Palmese). The images were reduced with astrometric calibration against Gaia DR3 (Gaia Collaboration 2020; Gaia Collaboration et al. 2021; L. Lindegren et al. 2021) and photometric calibration against PS1. We use SFFT (L. Hu et al. 2022) for image subtraction against archival DECam images (L. Hu et al. 2025, in preparation). We clearly resolve the rise in all filters; see X. J. Hall et al. (2025a) for more details.

HCT. We observed the transient with the 2.0 m HCT at the Indian Astronomical Observatory, obtaining multiple exposures in the Sloan Digital Sky Survey (SDSS) r' and i' filters, starting on 2025 September 9. Image subtraction was performed using the ZOGY-based Python pipeline (B. Zackay et al. 2016; H. Kumar et al. 2022a), with CFHT/MegaCam templates for r' and PS1 templates for i'. Basic reduction, astrometry, and PSF photometry followed the procedure described in H. Kumar et al. (2022b). The final magnitudes were calibrated against PS1.

Appendix B
Additional Candidate Vetting

In light of the superkilonova model, we reexamined the ZTF data with looser selection cuts, to identify any other young SNe that could potentially be linked to S250818k through the superkilonova model. Using the Python package emgwcave,[50] we conducted an archival search for all candidates within the 95% localization region of S250818k that were first detected by ZTF within 4 days of the GW trigger, had at least two ZTF detections, did not have host galaxy redshifts (photometric or spectroscopic) outside the 3D GW localization, and did not coincide with cataloged AGNs. We also rejected sources that did not show any substantial photometric variations in their ZTF photometry, to reject old SNe. In addition to ZTF 25abjmnps, we found six sources that are candidate infant SNe exploding around the time of the GW trigger. Next, we discuss each of these six sources in some detail, to assess whether any of them could be young stripped-envelope SNe consistent with the superkilonova model.

Two of these—ZTF 25abkoomo (SN 2025vfa; F. Forster et al. 2025; J. Johansson et al. 2025) and ZTF25 abjvflp (SN 2025uxs; K. C. Chambers et al. 2025a; J. Wise et al. 2025a)—have been spectroscopically classified as type Ia SNe. Thus, we reject these two thermonuclear explosions in the superkilonova picture.

ZTF 25abkeuac (SN 2025uic; D. O'Neill et al. 2025; J. Wise et al. 2025b) is a spectroscopically classified type II SN. Since it is not a stripped-envelope SN, we consider it to be unrelated in the superkilonova model.

ZTF 18aawigkf (SN 2025uso; K. C. Chambers et al. 2025b; J. Sollerman et al. 2025b; also reported in N. Franz et al. 2025; J. H. Gillanders et al. 2025) is a spectroscopically classified Type IIb SN. The first ZTF detection for this source is 3 days after the GW trigger, and we have ZTF nondetections of $g > 21.77$, $r > 21.83$ from MJD 60905.18 and 60905.23, respectively, corresponding to ($M_{g/r} \approx -14$). We fit the ZTF light curve with a power law to constrain the explosion time. The joint fit to the *g*-band and *r*-band light curve gives an explosion time estimate that is $2.27^{+0.31}_{-0.06}$ days after the GW trigger (the error bars are 3σ). Since the SN cannot explode after the kilonova in the superkilonova picture, we rule out association between SN 2025uso and S250818k.

ZTF 25abjvfjh (AT 2025wxt; J. Sollerman et al. 2025a) is an unclassified transient that was first detected 0.15 hr after the GW trigger and brightened by 2 mag over the next 20 days, before going into solar conjunction. This source has a photometric redshift of 0.134 ± 0.025 from SDSS, which is only marginally consistent with the 3σ limits from the GW detection. While we cannot conclusively exclude this transient, it is likely too distant to be associated with the GW trigger.

One other hostless transient, ZTF 25abjmput (AT 2025unk; R. Stein 2025b) has limited photometric data that show possible fading in its brightness. However, the age of this source cannot be determined, as no constraining nondetections exist for this source before its first detection. This source is

[49] https://github.com/CIERA-Transients/POTPyRI

[50] https://github.com/virajkaram/emgwcave

Table 1
All Rejected ZTF Candidate Counterparts to S250818k, alongside Their Primary Rejection Reason

ZTF Name	TNS Name	R.A. (deg)	Decl. (deg)	Rejection Reason
ZTF25abjmlzh	/	243.2441434	38.4684582	AGN
ZTF25abjmmee	/	239.2453486	40.1835372	AGN
…	…	…	…	…
ZTF25abjvfjt	/	235.8557562	24.3259834	BOGUS
ZTF25abjvfqi	/	234.0581773	24.3453163	BOGUS
…	…	…	…	…
ZTF25abjmotz	AT 2025uzg	233.7460861	24.8628222	FAR—specz = 0.229
ZTF25abjmmtx	AT 2025uzk	239.9571177	33.5514903	FAR—photz l95 = 0.139
ZTF25abjmmvx	AT 2025uzl	241.6009779	37.7817471	FAR—specz = 0.200
…	…	…	…	…
ZTF25abjmlwp	AT 2025unj	242.17952	40.0270559	OLD—FP
ZTF25abjmtcr	AT 2025uzr	241.442385	37.0062011	OLD—FP
…	…	…	…	…
ZTF25abjmnql	AT 2025uzi	244.8820228	36.804871	SLOW—$\delta g/\delta t = -0.20$ mag d^{-1}
ZTF25abjmotj	AT 2025uzj	233.5968358	23.1898252	SLOW—$\delta g/\delta t = -0.24$ mag d^{-1}
ZTF25abjmmub	/	239.9616469	40.4055308	STELLAR

Note. Candidates flagged as "AGNs" are nuclear and have AGN-like Wide-field Infrared Survey Explorer colors (D. Stern et al. 2005; E. L. Wright et al. 2010), are listed in Milliquas (E. W. Flesch 2023), or are classified as AGNs using DESI spectra (DESI Collaboration et al. 2025). Candidates flagged as "BOGUS" were noted as subtraction residuals based on manual visual vetting. Candidates flagged as "STELLAR" have a point-source counterpart in the reference image. AGN, STELLAR and BOGUS candidates were not reported to TNS. Candidates flagged as "FAR" are based on the host redshift—spectroscopic from DESI (DESI Collaboration et al. 2025) or SDSS (D. G. York et al. 2000) or photometric from Legacy Survey DR9 (https://www.legacysurvey.org/dr9)—being inconsistent with the GW volume. Candidates flagged as "OLD" are rejected based on detections recovered by forced photometry on ZTF data that precede the GW trigger time. Candidates rejected as "SLOW" are based on photometric evolution being slower than 0.3 mag day^{-1}. The rejection reasons are not mutually exclusive, so, for example, a FAR candidate could also be SLOW. Host galaxy spectra presented in X. J. Hall et al. (2025b). X. J. Hall (2025) more firmly rejects 2025uzf, 2025vaa, 2025uzx, 2025vad, 2025vat, 2025unn, 2025unm, 2025unl, 2025unk, 2025vak, and 2025vah as too far and not consistent with S250818k.

(This table is available in its entirety in machine-readable form in the online article.)

Table 2
Photometric Observations of AT2025ulz

Time (UT)	Phase	Mag (AB)	Δ_m	Limiting Mag	Filter	Instrument
2025-08-13 04:21:13	−4.87 days	/	/	21.2	ztfg	ZTF
2025-08-13 06:45:28	−4.77 days	/	/	20.2	ztfr	ZTF
2025-08-15 05:13:45	−2.84 days	/	/	21.0	ztfg	ZTF
2025-08-15 06:46:21	−2.77 days	/	/	20.6	ztfr	ZTF
2025-08-17 04:15:59	−0.88 day	/	/	21.1	ztfg	ZTF
2025-08-17 05:11:56	−0.84 day	/	/	21.0	ztfr	ZTF
2025-08-18 04:31:15	0.13 day	21.0	0.1	21.6	ztfg	ZTF
…	…	…	…	…	…	…
2025-09-21 03:25:08	34.09 days	23.1	0.1	25.0	sdssg	Binospec
2025-09-21 18:40:47	34.72 days	21.3	0.2	22.1	sdssi	FTW 3KK
2025-09-23 05:14:12	36.16 days	21.7	0.1	23.4	sdssz	GMOS
2025-09-23 05:25:04	36.17 days	21.7	0.1	23.2	sdssi	GMOS
2025-09-23 05:33:44	36.18 days	22.1	0.1	24.6	sdssr	GMOS
2025-09-23 05:42:26	36.18 days	22.9	0.1	24.6	sdssg	GMOS

Note. No magnitude is given in the case of nondetections or marginal detections below the nominal image depth, with the upper limit being given by the 5σ limiting magnitude. The phase is given relative to the merger time. Table 2 is published in its entirety in machine-readable format. A portion is shown here for guidance regarding its form and content.

(This table is available in its entirety in machine-readable form in the online article.)

consistent with being a late-time fading SN, and it is likely unrelated to the superkilonova picture.

In addition to these six sources discussed above that were flagged in our reanalysis, we also comment on two other sources —AT2025uow and AT2025uxu—reported by N. Franz et al. (2025) as sources with higher rank than AT2025ulz. AT 2025uxu was detected by ZTF and included in our candidate vetting, but it was ruled out due to a photometric redshift of $z \approx 0.102$ of its host galaxy from C. Saulder et al. (2023). AT 2025uow is too far south and was not covered by ZTF

observations. However, as noted in N. Franz et al. (2025), there is an ATLAS predetection 2 days before the GW trigger, which would rule it out in the superkilonova picture.

In summary, our reanalysis indicates that ZTF 25abjmnps (AT2025ulz) remains the only plausible candidate counterpart to S250818k in the superkilonova picture.

ORCID iDs

Mansi M. Kasliwal https://orcid.org/0000-0002-5619-4938
Tomás Ahumada https://orcid.org/0000-0002-2184-6430
Robert Stein https://orcid.org/0000-0003-2434-0387
Viraj Karambelkar https://orcid.org/0000-0003-2758-159X
Xander J. Hall https://orcid.org/0000-0002-9364-5419
Avinash Singh https://orcid.org/0000-0003-2091-622X
Christoffer Fremling https://orcid.org/0000-0002-4223-103X
Brian D. Metzger https://orcid.org/0000-0002-4670-7509
Mattia Bulla https://orcid.org/0000-0002-8255-5127
Vishwajeet Swain https://orcid.org/0000-0002-7942-8477
Sarah Antier https://orcid.org/0000-0002-7686-3334
Marion Pillas https://orcid.org/0000-0003-3224-2146
Malte Busmann https://orcid.org/0009-0001-0574-2332
James Freeburn https://orcid.org/0009-0006-7990-0547
Sergey Karpov https://orcid.org/0000-0003-0035-651X
Aleksandra Bochenek https://orcid.org/0009-0008-2714-2507
Brendan O'Connor https://orcid.org/0000-0002-9700-0036
Daniel A. Perley https://orcid.org/0000-0001-8472-1996
Dalya Akl https://orcid.org/0009-0006-4358-9929
Shreya Anand https://orcid.org/0000-0003-3768-7515
Andrew Toivonen https://orcid.org/0009-0008-9546-2035
Sam Rose https://orcid.org/0000-0003-4725-4481
Theophile Jegou du Laz https://orcid.org/0009-0003-6181-4526
Chang Liu https://orcid.org/0000-0002-7866-4531
Kaustav Das https://orcid.org/0000-0001-8372-997X
Sushant Sharma Chaudhary https://orcid.org/0000-0003-1314-4241
Tyler Barna https://orcid.org/0000-0002-4843-345X
Aditya Pawan Saikia https://orcid.org/0009-0005-2987-0688
Igor Andreoni https://orcid.org/0000-0002-8977-1498
Eric C. Bellm https://orcid.org/0000-0001-8018-5348
Varun Bhalerao https://orcid.org/0000-0002-6112-7609
S. Bradley Cenko https://orcid.org/0000-0003-1673-970X
Michael W. Coughlin https://orcid.org/0000-0002-8262-2924
Daniel Gruen https://orcid.org/0000-0003-3270-7644
Daniel Kasen https://orcid.org/0000-0002-5981-1022
Adam A. Miller https://orcid.org/0000-0001-9515-478X
Samaya Nissanke https://orcid.org/0000-0001-6573-7773
Antonella Palmese https://orcid.org/0000-0002-6011-0530
Jesper Sollerman https://orcid.org/0000-0003-1546-6615
G.C. Anupama https://orcid.org/0000-0003-3533-7183
Smaranika Banerjee https://orcid.org/0000-0001-6595-2238
Sudhanshu Barway https://orcid.org/0000-0002-3927-5402
Joshua S. Bloom https://orcid.org/0000-0002-7777-216X
Tomás Cabrera https://orcid.org/0000-0002-1270-7666
Tracy Chen https://orcid.org/0000-0001-9152-6224
Chris Copperwheat https://orcid.org/0000-0001-7983-8698
Alessandra Corsi https://orcid.org/0000-0001-8104-3536
Richard Dekany https://orcid.org/0000-0002-5884-7867
Nicholas Earley https://orcid.org/0000-0001-6627-9903
Matthew Graham https://orcid.org/0000-0002-3168-0139
Patrice Hello https://orcid.org/0009-0000-7527-205X
George Helou https://orcid.org/0000-0003-3367-3415
Lei Hu https://orcid.org/0000-0001-7201-1938
Yves Kini https://orcid.org/0000-0002-0428-8430
Ashish Mahabal https://orcid.org/0000-0003-2242-0244
Frank Masci https://orcid.org/0000-0002-8532-9395
Tanishk Mohan https://orcid.org/0009-0001-4683-388X
Natalya Pletskova https://orcid.org/0009-0008-8062-445X
Josiah Purdum https://orcid.org/0000-0003-1227-3738
Yu-Jing Qin https://orcid.org/0000-0003-3658-6026
Nabeel Rehemtulla https://orcid.org/0000-0002-5683-2389
Anirudh Salgundi https://orcid.org/0000-0003-3173-4691
Yuankun Wang https://orcid.org/0000-0001-5538-0395

References

Abbasi, R., Ackermann, M., Adams, J., et al. 2022, PhRvD, 106, 022005
Abbott, B. P., Abbott, R., Abbott, T. D., et al. 2016, PhRvL, 116, 061102
Abbott, B. P., Abbott, R., Abbott, T. D., et al. 2017a, ApJL, 848, L12
Abbott, B. P., Abbott, R., Abbott, T. D., et al. 2017b, PhRvL, 119, 161101
Abbott, R., Abbott, T. D., Acernese, F., et al. 2022, PhRvL, 129, 061104
Agudo, I., Amati, L., An, T., et al. 2023, A&A, 675, A201
Ahumada, T., Anand, S., Bulla, M., et al. 2025, arXiv:2507.00357
Ahumada, T., Anand, S., Coughlin, M. W., et al. 2024, PASP, 136, 114201
Alléné, C., Aubin, F., Bentara, I., et al. 2025, CQGra, 42, 105009
Almualla, M., Coughlin, M. W., Anand, S., et al. 2020, MNRAS, 495, 4366
Andreoni, I., Coughlin, M. W., Criswell, A. W., et al. 2024, APh, 155, 102904
Andreoni, I., Coughlin, M. W., Kool, E. C., et al. 2021, ApJ, 918, 63
Andreoni, I., Goldstein, D. A., Kasliwal, M. M., et al. 2020, ApJ, 890, 131
Andreoni, I., Margutti, R., Salafia, O. S., et al. 2022, ApJS, 260, 18
Barnes, J., & Duffell, P. C. 2023, ApJ, 952, 96
Becker, A., 2015 HOTPANTS: High Order Transform of PSF ANd Template Subtraction, Astrophysics Source Code Library, ascl:1504.004
Bellm, E. C., Kulkarni, S. R., Graham, M. J., et al. 2019, PASP, 131, 018002
Bersten, M. C., Benvenuto, O. G., Nomoto, K., et al. 2012, ApJ, 757, 31
Bertin, E. 2006, ASPC, 351, 112
Bertin, E., & Arnouts, S. 1996, A&AS, 117, 393
Bertin, E., Mellier, Y., Radovich, M., et al. 2002, ASPC, 281, 228
Blagorodnova, N., Neill, J. D., Walters, R., et al. 2018, PASP, 130, 035003
Bulla, M. 2019, MNRAS, 489, 5037
Bulla, M. 2023, MNRAS, 520, 2558
Busmann, M., O'Connor, B., Sommer, J., et al. 2025, A&A, 701, A225
Cabrera, T., Palmese, A., Hu, L., et al. 2024, PhRvD, 110, 123029
Cantiello, M., Yoon, S. C., Langer, N., & Livio, M. 2007, A&A, 465, L29
Carr, B. J. 1975, ApJ, 201, 1
Chambers, K. C., Boer, T. D., Fairlamb, J., et al. 2025a, TNSTR 2025–3320,
Chambers, K. C., Boer, T. D., Fairlamb, J., et al. 2025b, TNSTR 2025-3300,
Chambers, K. C., Magnier, E. A., Metcalfe, N., et al. 2016, arXiv:1612.05560
Chapline, G. F. 1975, Natur, 253, 251
Chaudhary, S. S., Toivonen, A., Waratkar, G., et al. 2024, PNAS, 121, e2316474121
Chen, Y.-X., & Metzger, B. D. 2025, ApJL, 991, L22
Coughlin, M. W., Antier, S., Corre, D., et al. 2019, MNRAS, 489, 5775
Coughlin, M. W., Bloom, J. S., Nir, G., et al. 2023, ApJS, 267, 31
Coughlin, M. W., Tao, D., Chan, M. L., et al. 2018, MNRAS, 478, 692
Coulter, D. A., Foley, R. J., Kilpatrick, C. D., et al. 2017, Sci, 358, 1556
Criswell, A. W., Leggio, S. C., Coughlin, M. W., et al. 2025, PASP, 137, 054101
Das, K. K., Kasliwal, M. M., Fremling, C., et al. 2025, PASP, 137, 044203
Davies, M. B., King, A., Rosswog, S., & Wynn, G. 2002, ApJL, 579, L63
de Barra, C. 2025, GCN, 41441
de Jaeger, T., Shappee, B. J., Kochanek, C. S., et al. 2022, MNRAS, 509, 3427
Dekany, R., Smith, R. M., Riddle, R., et al. 2020, PASP, 132, 038001
DESI Collaboration, Abdul-Karim, M., Adame, A. G., et al. 2025, arXiv:2503.14745
Dey, A., Schlegel, D. J., Lang, D., et al. 2019, AJ, 157, 168
Dobie, D., Murphy, T., Kaplan, D. L., et al. 2021, MNRAS, 505, 2647
Dodici, M., & Tremaine, S. 2024, ApJ, 972, 193
Drout, M. R., Piro, A. L., Shappee, B. J., et al. 2017, Sci, 358, 1570
Durisen, R. H., & Tohline, J. E. 1985, in Protostars and Planets II, ed. D. C. Black & M. S. Matthews (Univ. of Arizona Press), 534
Ergon, M., Sollerman, J., Fraser, M., et al. 2014, A&A, 562, A17
Evans, P. A., Cenko, S. B., Kennea, J. A., et al. 2017, Sci, 358, 1565
Fabricant, D., Fata, R., Epps, H., et al. 2019, PASP, 131, 075004
Fitzpatrick, E. L. 1999, PASP, 111, 63
Flesch, E. W. 2023, OJAp, 6, 49
Forster, F., Bauer, F. E., Pignata, G., et al. 2025, TNSTR 2025–3330,
Franz, N., Subrayan, B., Kilpatrick, C. D., et al. 2025, arXiv:2510.17104

Gaia Collaboration 2020, yCat, 1350, 0
Gaia Collaboration, Brown, A. G. A., Vallenari, A., et al. 2021, A&A, 649, A1
Gammie, C. F. 2001, ApJ, 553, 174
Ghirlanda, G., Salafia, O. S., Paragi, Z., et al. 2019, Sci, 363, 968
Gillanders, J. H., Huber, M. E., Nicholl, M., et al. 2025, arXiv:2510.01142
Goodman, J., & Tan, J. C. 2004, ApJ, 608, 108
Gössl, C. A., & Riffeser, A. 2002, A&A, 381, 1095
Govreen-Segal, T., & Nakar, E. 2023, MNRAS, 524, 403
Graham, M. J., Ford, K. E. S., McKernan, B., et al. 2020, PhRvL, 124, 251102
Graham, M. J., Kulkarni, S. R., Bellm, E. C., et al. 2019, PASP, 131, 078001
Graham, M. J., McKernan, B., Ford, K. E. S., et al. 2023, ApJ, 942, 99
Haensel, P., Zdunik, J. L., & Douchin, F. 2002, A&A, 385, 301
Hall, X. J. 2025, AT2025ulz and S250818k: Leveraging DESI spectroscopy in the hunt for a kilonova associatedwith a sub-solar mass gravitational wave candidate, v2, Zenodo, doi:10.5281/zenodo.17451484
Hall, X. J., Busmann, M., Koehn, H., et al. 2025a, arXiv:2510.24620
Hall, X. J., Palmese, A., O'Connor, B., et al. 2025b, arXiv:2510.23723
Hallinan, G., Corsi, A., Mooley, K. P., et al. 2017, Sci, 358, 1579
Hallinan, G., Ravi, V., Weinreb, S., et al. 2019, BAAS, 51, 255
Hanna, C., Kennington, J., Niu, W., et al. 2025, PhRvD, 112, 044013
Hawking, S. 1971, MNRAS, 152, 75
Hearty, F. R., Morse, J., Beland, S., et al. 2004, SPIE, 5492, 1623
Hopp, U., Bender, R., Grupp, F., et al. 2014, SPIE, 9145, 91452D
Hu, L., Cabrera, T., Palmese, A., et al. 2025, ApJL, 990, L46
Hu, L., Wang, L., Chen, X., & Yang, J. 2022, ApJ, 936, 157
IceCube Collaboration, Aartsen, M. G., Ackermann, M., et al. 2018, Sci, 361, eaat1378
IceCube Collaboration, Abbasi, R., Ackermann, M., et al. 2022, Sci, 378, 538
Icecube Collaboration, Abbasi, R., Ackermann, M., et al. 2023, Sci, 380, 1338
Imshennik, V. S., & Popov, D. V. 1998, AstL, 24, 206
Ivezić, Ž., Kahn, S. M., Tyson, J. A., et al. 2019, ApJ, 873, 111
Jermyn, A. S., Bauer, E. B., Schwab, J., et al. 2023, ApJS, 265, 15
Johansson, J., Mehla, A., Chu, M., & Fremling, C. 2025, TNSCR, 2025–3834
Kadler, M., Krauß, F., Mannheim, K., et al. 2016, NatPh, 12, 807
Kaiser, N., Burgett, W., Chambers, K., et al. 2010, SPIE, 7733, 77330E
Karpov, S. 2025, AcPol, 65, 50
Kasen, D., Badnell, N. R., & Barnes, J. 2013, ApJ, 774, 25
Kasen, D., Metzger, B., Barnes, J., Quataert, E., & Ramirez-Ruiz, E. 2017, Natur, 551, 80
Kasliwal, M. M., Anand, S., Ahumada, T., et al. 2020, ApJ, 905, 145
Kasliwal, M. M., Earley, N., Smith, R., et al. 2025, PASP, 137, 065001
Kasliwal, M. M., Nakar, E., Singer, L. P., et al. 2017, Sci, 358, 1559
Kulkarni, S. R., Harrison, F. A., Grefenstette, B. W., et al. 2021, arXiv:2111.15608
Kumar, H., Bhalerao, V., Anupama, G. C., et al. 2022a, MNRAS, 516, 4517
Kumar, H., Bhalerao, V., Anupama, G. C., et al. 2022b, AJ, 164, 90
Labrie, K., Anderson, K., Cárdenes, R., Simpson, C., & Turner, J. E. H. 2019, ASPC, 523, 321
Lang-Bardl, F., Bender, R., Goessl, C., et al. 2016, SPIE, 9908, 990844
Lerner, Y., Stone, N. C., & Ofengeim, D. D. 2025, arXiv:2505.21617
Li, W., Leaman, J., Chornock, R., et al. 2011, MNRAS, 412, 1441
Ligo Scientific CollaborationVIRGO CollaborationKagra Collaboration, et al. 2025, GCN, 41437, 1
Lindegren, L., Klioner, S. A., Hernández, J., et al. 2021, A&A, 649, A2
Liu, C., & Miller, A. A. 2025, arXiv:2508.15278
Liu, Y.-Q., Modjaz, M., Bianco, F. B., & Graur, O. 2016, ApJ, 827, 90
Lohev, N., Sabach, E., Gilkis, A., & Soker, N. 2019, MNRAS, 490, 9
Long, G. 2022, The formation of the stripped envelope type IIb Supernova progenitors: Rotation, Metallicity and Overshooting, v10398, Zenodo, doi:10.5281/zenodo.6578992
Long, G., Song, H., Meynet, G., et al. 2022, ApJS, 262, 26
LVK Collaboration, Abbott, R., Abe, H., et al. 2023, MNRAS, 524, 5984
Margutti, R., Berger, E., Fong, W., et al. 2017, ApJL, 848, L20
Masci, F. J., Laher, R. R., Rusholme, B., et al. 2019, PASP, 131, 018003
McLean, I. S., Steidel, C. C., Epps, H. W., et al. 2012, SPIE, 8446, 84460J
Metzger, B. D., Hui, L., & Cantiello, M. 2024, ApJL, 971, L34
Modjaz, M., Liu, Y. Q., Bianco, F. B., & Graur, O. 2016, ApJ, 832, 108
Mooley, K. P., Anderson, J., & Lu, W. 2022, Natur, 610, 273
Mooley, K. P., Deller, A. T., Gottlieb, O., et al. 2018, Natur, 561, 355
Morales-Garoffolo, A., Elias-Rosa, N., Benetti, S., et al. 2014, MNRAS, 445, 1647
Morozova, V., Piro, A. L., Renzo, M., et al. 2015, ApJ, 814, 63
Müller, B., Heger, A., & Powell, J. 2025, PhRvL, 134, 071403
Nakar, E. 2020, PhR, 886, 1
Nedora, V., Bernuzzi, S., Radice, D., et al. 2021, ApJ, 906, 98
Nesvorný, D., Youdin, A. N., & Richardson, D. C. 2010, AJ, 140, 785
Nicholl, M., & Andreoni, I. 2025, RSPTA, 383, 20240126
Niu, W., Hanna, C., Haster, C.-J., et al. 2025, arXiv:2509.09741
Nomoto, K., & Kondo, Y. 1991, ApJL, 367, L19
Nomoto, K., Suzuki, T., Shigeyama, T., et al. 1993, Natur, 364, 507
O'Connor, B., Ricci, R., Troja, E., et al. 2025, arXiv:2510.23728
Oke, J. B., Cohen, J. G., Carr, M., et al. 1995, PASP, 107, 375
O'Neill, D., Ackley, K., Dyer, M., et al. 2025, TNSTR, 2025–3243
Pang, P. T. H., Dietrich, T., Coughlin, M. W., et al. 2023, NatCo, 14, 8352
Paterson, K., Lundquist, M. J., Rastinejad, J. C., et al. 2021, ApJ, 912, 128
Paxton, B., Bildsten, L., Dotter, A., et al. 2011, ApJS, 192, 3
Paxton, B., Cantiello, M., Arras, P., et al. 2013, ApJS, 208, 4
Paxton, B., Marchant, P., Schwab, J., et al. 2015, ApJS, 220, 15
Paxton, B., Schwab, J., Bauer, E. B., et al. 2018, ApJS, 234, 34
Paxton, B., Smolec, R., Schwab, J., et al. 2019, ApJS, 243, 10
Peng, C. Y., Ho, L. C., Impey, C. D., & Rix, H.-W. 2002, AJ, 124, 266
Perley, D. A. 2019, PASP, 131, 084503
Pessi, T., Desai, D. D., Prieto, J. L., et al. 2025, A&A, 703, A34
Pian, E., D'Avanzo, P., Benetti, S., et al. 2017, Natur, 551, 67
Piro, A. L., & Pfahl, E. 2007, ApJ, 658, 1173
Plavin, A., Kovalev, Y. Y., Kovalev, Y. A., & Troitsky, S. 2020, ApJ, 894, 101
Postnov, K. A., Kuranov, A. G., Kolesnikov, D. A., Popov, S. B., & Porayko, N. K. 2016, MNRAS, 463, 1642
Poznanski, D., Prochaska, J. X., & Bloom, J. S. 2012, MNRAS, 426, 1465
Prochaska, J., Hennawi, J., Westfall, K., et al. 2020, JOSS, 5, 2308
Radice, D., Perego, A., Hotokezaka, K., et al. 2018, ApJ, 869, 130
Reusch, S., Stein, R., Kowalski, M., et al. 2022, PhRvL, 128, 221101
Saulder, C., Howlett, C., Douglass, K. A., et al. 2023, MNRAS, 525, 1106
Schlafly, E. F., & Finkbeiner, D. P. 2011, ApJ, 737, 103
Serra-Ricart, M., Alarcón, M. R., Licandro, J., & Abárzuza, F. 2024, EPSC, 17, EPSC2024
Shivkumar, H., Jaodand, A. D., Balasubramanian, A., et al. 2023, ApJ, 952, 86
Shivvers, I., Filippenko, A. V., Silverman, J. M., et al. 2019, MNRAS, 482, 1545
Siegel, D. M., Agarwal, A., Barnes, J., et al. 2022, ApJ, 941, 100
Skrutskie, M. F., Cutri, R. M., Stiening, R., et al. 2006, AJ, 131, 1163
Smartt, S. J., Chen, T.-W., Jerkstrand, A., et al. 2017, Natur, 551, 75
Smartt, S. J., Gillanders, J. H., Huber, M. E., et al. 2025, GCN, 41493, 1
Soares-Santos, M., Holz, D. E., Annis, J., et al. 2017, ApJL, 848, L16
Sollerman, J., Fremling, C., Perley, D., & Laz, T. D. 2025a, TNSTR 2025–3580,
Sollerman, J., Mehla, A., Chu, M., & Fremling, C. 2025b, TNSCR 2025–3920,
Sravan, N., Marchant, P., Kalogera, V., Milisavljevic, D., & Margutti, R. 2020, ApJ, 903, 70
Steele, I. A., Smith, R. J., Rees, P. C., et al. 2004, SPIE, 5489, 679
Stein, R. 2025a, TNSTR 2025–3264,
Stein, R. 2025b, TNSTR 2025–3282,
Stein, R., Ahumada, T., Kasliwal, M., et al. 2025b, GCN, 41414
Stein, R., Ho, A. Y. Q., Gangopadhyay, A., et al. 2025a, arXiv:2508.08355
Stein, R., Reusch, S., Franckowiak, A., et al. 2023, MNRAS, 521, 5046
Stein, R., van Velzen, S., Kowalski, M., et al. 2021, NatAs, 5, 510
Stern, D., Eisenhardt, P., Gorjian, V., et al. 2005, ApJ, 631, 163
Stein, R. D., Reusch, S., & Necker, J., 2025 desy-multimessenger/nuztf, v3.0.0, Zenodo, doi:10.5281/zenodo.14990431
Stritzinger, M. D., Taddia, F., Burns, C. R., et al. 2018, A&A, 609, A135
Swain, V., Ahumada, T., Patil, S. K., et al. 2025, arXiv:2509.02769
Taddia, F., Stritzinger, M. D., Bersten, M., et al. 2018, A&A, 609, A136
Tanvir, N. R., Levan, A. J., González-Fernández, C., et al. 2017, ApJL, 848, L27
The LIGO Scientific CollaborationThe Virgo Collaborationthe KAGRA Collaboration 2025, arXiv:2508.18082
Toomre, A. 1964, ApJ, 139, 1217
Troja, E., Piro, L., van Eerten, H., et al. 2017, Natur, 551, 71
Tsuna, D., Fuller, J., & Lu, W. 2025, arXiv:2508.21116
van der Walt, S. J., Crellin-Quick, A., & Bloom, J. S. 2019, JOSS, 4, 1247
Wang, H., Dastidar, R. G., Giannios, D., & Duffell, P. C. 2024, ApJS, 273, 17
Weisenburger, K. L., Huehnerhoff, J., Levesque, E. M., & Massey, P. 2017, JOSS, 2, 102
Wise, J., Covarrubias, S., Chu, M., & Fremling, C. 2025a, TNSCR 2025–3869,
Wise, J., Mehla, A., Chu, M., & Fremling, C. 2025b, TNSCR 2025–3625,
Woosley, S. E., Eastman, R. G., Weaver, T. A., & Pinto, P. A. 1994, ApJ, 429, 300
Wright, E. L., Eisenhardt, P. R. M., Mainzer, A. K., et al. 2010, AJ, 140, 1868
Yang, Y.-H., Troja, E., Ristić, M., et al. 2025, arXiv:2510.18854
Yoon, S.-C., Chun, W., Tolstov, A., Blinnikov, S., & Dessart, L. 2019, ApJ, 872, 174
Yoon, S.-C., Dessart, L., & Clocchiatti, A. 2017, ApJ, 840, 10
York, D. G., Adelman, J., Anderson, J. E., Jr., et al. 2000, AJ, 120, 1579
Zackay, B., Ofek, E. O., & Gal-Yam, A. 2016, ApJ, 830, 27
Zel'dovich, Y. B., & Novikov, I. D. 1967, SvA, 10, 602